

1 Effective energy controls on flocculation under various  
2 wave-current regimes

3 Rafael Ramírez-Mendoza<sup>a,b</sup>, Alejandro J. Souza<sup>b</sup>, Laurent O. Amoudry<sup>b</sup>,  
4 Andrew J. Plater<sup>c</sup>

5 <sup>a</sup>*CICESE, Carr. Eda.-Tij. No. 3918, Playitas, Eda., BC, 22860, México*

6 <sup>b</sup>*National Oceanography Centre*

7 *6 Brownlow Street, Joseph Proudman Building, Liverpool, United Kingdom, L3 5DA*

8 <sup>c</sup>*Department of Geography, University of Liverpool*

9 *Roxby Building, L69 7ZT, UK*

---

10 **Abstract**

11 Transport of sediments is a critical process in the coastal zone because  
12 of its relation with coastal erosion, productivity and pollution. Of particular  
13 interest are the dynamics of suspended cohesive sediments, known as flocs,  
14 which can aggregate and break-up during the flocculation process. This  
15 changes their size, density, settling velocity and overall transport. Even  
16 though turbulence is widely accepted to be an important control on floc  
17 aggregation and break-up, specific and detailed floc behaviour is still not  
18 fully understood. The present study seeks to help in the understanding of  
19 the intra-tidal turbulence-induced flocculation under different current-wave  
20 regimes. Observations of floc size and currents at high sample rates are used  
21 to investigate the changes throughout a fortnightly cycle. The occurrence  
22 of waves at different stages during the sampling period enabled determina-  
23 tion of three regimes of currents dominant, combined waves and currents,  
24 and wave dominant. The first two regimes showed quarter-diurnal floc size  
25 variability with aggregation during low turbulence (slack waters) and higher

26 flocculation magnitude on low water slack. Break-up occurred with high  
27 turbulence (flood and ebb) with higher magnitude after ebb. During the  
28 “currents-waves” regime, waves were tidally modulated and led to enhanced  
29 aggregation and break-up, with larger flocculation size range than during the “current  
30 dominant” regime. Wave tidal modulation and quarter-diurnal variability of  
31 flocculation size were lost when waves were dominant. Flocculation sizes exhibited a low  
32 range related to wave height. Inverse relationships between turbulent prop-  
33 erties and median flocculation size were found for the three regimes, with higher  
34 scatter of data for the Kolmogorov microscale and shear rate due to different  
35 flocculation behaviour during flood and ebb phases. Effective kinetic energy obtained  
36 from the combined effect of both currents and waves seems to have a bet-  
37 ter relationship with flocculation size, which suggests its use as a flocculation size predictor  
38 instead of shear stress.

39 *Keywords:*

40 Flocculation, turbulence, waves, currents, sediments

---

## 41 **1. Introduction**

42 The dynamics of suspended sediment play an important role in estuarine  
43 systems as they are strongly related to accretion, erosion, estuarine turbid-  
44 ity maxima, primary productivity, pollution and overall estuarine budgets.  
45 A key characteristic of estuarine sediments is the presence of fine cohesive  
46 sediments, which may aggregate or break-up via the so-called flocculation  
47 process. The resulting suspended particulate aggregates, known as flocs,  
48 display time and space varying characteristics, such as size, density, and set-  
49 tling velocity and therefore influence the overall estuarine sediment transport

50 (Winterwerp and van Kesteren, 2004). Knowledge of the physical processes  
51 that control flocculation is crucial toward good management, sustainability  
52 of the resources, and conservation of natural ecosystems where fine sediments  
53 are important.

54 A number of field and laboratory studies have highlighted relationships  
55 between floc size, floc settling velocity, current shear stress and concentration,  
56 which have been summarized in the well known conceptual diagram by Dyer  
57 (1989). An increase in shear stress from rest initially enhances floc aggrega-  
58 tion through an increase in particle collisions. As shear stress continues to  
59 increase, flocs reach a maximum size and break-up becomes the most impor-  
60 tant effect causing a reduction in floc size. This behaviour is also modulated  
61 by sediment concentration because of the increase in inter-particle collisions  
62 and also increases the probability of aggregation. The diagram by Dyer has  
63 been confirmed by a number of experiments (van Leussen, 1994; Manning and  
64 Dyer, 1999; Verney et al., 2011) and field observations (Fettweis et al., 2006;  
65 Braithwaite et al., 2012). However, this conceptual diagram only provides a  
66 simplified and partial understanding of the processes involved in flocculation.  
67 Indeed, in natural environments, flocculation is also impacted by a range of  
68 additional factors, such as hysteresis due to different time scales of aggre-  
69 gation and break-up (Verney et al., 2011), spatial variability (van Leussen,  
70 1999; Fugate and Friedrichs, 2003), physico-chemical and biological effects  
71 van Leussen (1999), and sediment provenance (Jago and Jones, 1998; Bass  
72 et al., 2002; Fettweis et al., 2012).

73 Floc behaviour has been included in models via floc size and settling rate  
74 relationships of varying complexity (e.g., Winterwerp, 2002; Maerz et al.,

75 2011; Maggi, 2007). Validation of such models relies on long-term measure-  
76 ments of floc size, which remain scarce, and of settling velocities, which are  
77 difficult to measure *in situ*. In contrast to measurements based on settling  
78 columns which can disrupt the flocs and only work for low concentrations  
79 (free falling flocs), reliable floc sizes can be measured *in situ* using video  
80 images (Mikkelsen et al., 2006; Graham and Nimmo-Smith, 2010; Reynolds  
81 et al., 2010) and light diffraction techniques (Agrawal and Pottsmith, 2000;  
82 Reynolds et al., 2010; Davies et al., 2012). Formulations can then be used  
83 to obtain settling rates, such as the widely applied formula by Winterwerp  
84 (1998) which uses the floc diameter and fractal theory. Even though using  
85 fractal theory introduces complexity via an additional unknown factor (e.g.,  
86 Camenen, 2009), there is, to date, no other method to deal with the floc  
87 complex structures.

88 Nevertheless, proposed formulations are still not capable of reproducing  
89 the wide scattering of the relationship between floc size and settling velocity.  
90 This is clearly observed in the compilations of different studies by Khelifa and  
91 Hill (2006) and Strom and Keyvani (2011) where plots of floc size against  
92 settling velocity show high data dispersion and low correlation coefficient  
93 values. This scattering seems to be strongly related to hydrodynamic con-  
94 ditions at temporal scales from intra-tidal to spring-neap cycles in addition  
95 to the factors mentioned previously. Indeed, flocculation is related to energy  
96 conditions from different hydrodynamic regimes as strong currents typically  
97 favour floc fragmentation while weak currents enhance floc aggregation. This  
98 behaviour is affected by kinetic energy differences between spring and neap  
99 tides, asymmetries during flood and ebb tidal phases, and sediment consoli-

100 dation during neap tides (e.g. Mehta, 1988; Sanford and Maa, 2001; Dankers  
101 and Winterwerp, 2007).

102 In addition, the impact of the combination of both currents and waves  
103 on the flocculation process is still not well known. Waves alone can cause  
104 seabed erosion and liquefaction which may have effects on the water column  
105 floc concentration. Bed shear stress also increases with the presence of both  
106 currents and waves (Soulsby, 1993) leading to changes in floc concentrations.  
107 We therefore still require a better understanding of the relationship between  
108 particle behaviour and turbulence under different hydrodynamic (waves and  
109 currents) conditions, in order to obtain better predictions of sediment trans-  
110 port in estuaries.

111 The present study seeks to improve our understanding of floc behaviour  
112 under the effect of different hydrodynamic conditions. We hypothesize that,  
113 in spite of the stochastic nature of flocs (Winterwerp et al., 2006; Maggi,  
114 2008) and waves, scattering between turbulence and floc size can be reduced  
115 by using appropriate measures of turbulence under various hydrodynamic  
116 (i.e., combinations of waves and currents) regimes. Specifically, we propose  
117 the use of an effective kinetic energy instead of the widely used variables  
118 turbulence shear rate  $G$ , turbulent shear stress, or Kolmogorov microscale.  
119 To that end, we use *in situ* observations of floc size obtained from a LISST  
120 (Lasser In Situ Scattering and Transmisometry) and turbulence properties  
121 computed from high-frequency acoustic current meter data. Our case study  
122 enabled a comparison between three distinct hydrodynamic regimes: weak  
123 currents in absence of waves, combined effect of waves and currents, and  
124 dominant wave forcing. The observations are also split depending on tidal

125 phase (flood versus ebb), which is found to have a significant impact on the  
126 scattering between turbulence and floc size.

127 We describe the case study location in the next section and the observa-  
128 tional methods in section 3. Results are presented in section 4, their interpre-  
129 tation and discussion in section 5. Finally the main findings are summarised  
130 in the conclusion.

## 131 **2. Study area**

132 Observations for this study were carried out in the Welsh Channel, one  
133 of the two channels connecting the Dee Estuary to the Liverpool Bay in the  
134 United Kingdom (Fig. 1). The Dee is a funnel shaped coastal plain estuary  
135 with a channel that bifurcates into the Welsh and Hilbre channels before  
136 entering Liverpool Bay (Fig. 1c). Most of the inner estuary remains very  
137 shallow with only the central channel at a depth of about 5 m below mean  
138 sea level. Depth then increases from the inner estuary towards the channels  
139 to 22 and 24 m for Hilbre and Welsh respectively. The channels finish with  
140 depths diminishing to less than 5 m depth in the outer part of the estuary.

141 The Dee is tidally dominated with a tidal range of about 10 m during  
142 spring tides and currents of more than  $1 \text{ m}\cdot\text{s}^{-1}$  on the surface and nearly  $0.5$   
143  $\text{m}\cdot\text{s}^{-1}$  near the seabed (Bolaños et al., 2013). Tides are significantly distorted  
144 due to the shallow nature of the estuary and tidal asymmetry results in flood  
145 dominance on sandy and muddy shallow areas, and weaker ebb dominance  
146 in the channels (Moore et al., 2009). In spite of the low river discharge,  
147 baroclinic behaviour remains important in the estuary, with stratification,  
148 tidal straining, wind and friction all having a role in the hydrodynamics of

149 both channels (Bolaños et al., 2013). Nevertheless, the residual spring tide is  
150 more important for the circulation of the Welsh Channel, while baroclinicity  
151 is more important for the circulation of the Hilbre Channel (Brown et al.,  
152 2014).

153 Suspended sediment concentrations increase from the Liverpool Bay to  
154 the inner part of the Dee estuary where muddy bed sediments prevail. Obser-  
155 vations of suspended sediment concentration to the northwest of the estuary  
156 entrance, still in the Liverpool Bay, were of about  $24 \text{ mg}\cdot\text{l}^{-1}$  in winter and  $5$   
157  $\text{mg}\cdot\text{l}^{-1}$  in summer with size of about  $100 \mu\text{m}$  for both suspended sediments  
158 at the surface and near the bottom (Krivtsov et al., 2008). At the entrance  
159 of the estuary, in the Hilbre Channel, Amoudry et al. (2014) reported maxi-  
160 mum suspended sediment concentration of  $500 \text{ mg}\cdot\text{l}^{-1}$  and Bolaños and Souza  
161 (2010) found dominance of fine flocs of about  $70 \mu\text{m}$  in both channels. Inside  
162 the estuary, early measurements from bed samples by Turner et al. (1994)  
163 showed that the sediment fraction below  $63 \mu\text{m}$  was present in percentages  
164 between 23% and 62%.

165 Because of the tidal dominance, SPM concentrations in the Dee Estuary  
166 are controlled by a combination of tidal advection and resuspension (Bolaños  
167 et al., 2009). The levels of accretion in the estuary indicate the Dee is a  
168 depository of sediments (Moore et al., 2009) with the sediment identified to  
169 mostly be of marine origin (Turner et al., 1994) which is in agreement with  
170 observations and modelling results that show bottom currents and sediment  
171 transport from the Liverpool Bay to the estuary entrance (e.g. Halliwell,  
172 1973; Simpson and Sharples, 1991; Polton et al., 2011; Souza and Lane, 2013).  
173 However, according to Holden et al. (2011), it is possible that sediments

174 from the estuary contribute to the accretion of the Sefton coast to the north  
175 of the Dee. In addition, results by Moore et al. (2009) show a decrease  
176 in accretion rates which means the estuary is nearly in geomorphological  
177 equilibrium. The sediment transport in the estuary is not well known and  
178 is further complicated because of the presence of fine sediments leading to  
179 cohesive behaviour.

180 The dynamics of suspended sediments in the Dee estuary seems to mostly  
181 depend on turbulence, spatial distribution and biological factors. Classical  
182 links between turbulent properties and flocs in the Dee Estuary following  
183 which aggregation occurs during periods of weak turbulence (slack water  
184 at low and high tide) and break-up during periods of intense turbulence  
185 (maximum flood or ebb current) have been reported (e.g., Thurston, 2009;  
186 Ramírez-Mendoza et al., 2014) and included in numerical models (Ramírez-  
187 Mendoza et al., 2014). Amoudry et al. (2014) highlighted the importance  
188 of horizontal gradients in suspended sediment, themselves due to gradients  
189 in turbulence and bed sediment distribution, toward reproducing observed  
190 SPM behaviour in the Hilbre Channel.

### 191 **3. Methodology**

#### 192 *3.1. Observations*

193 Observations for the present investigation were taken using a LISST  
194 (Laser In-Situ Scattering and Transmissometry) and an ADV (Acoustic Doppler  
195 Velocimeter) deployed in a tripod in the Welsh channel from 12 February to  
196 8 March in 2008 at 1.5 and 0.3 metres above bottom, respectively. Details  
197 of the mooring and deployment can be found in Bolaños and Souza (2010).

198 The LISST uses laser diffraction techniques to measure floc sizes between  
199 2.5-500  $\mu m$  and their corresponding volume concentrations (Agrawal and  
200 Pottsmith, 2000). For this study, the LISST recorded one sample every 40  
201 seconds during a 20-minute period every hour. Data were then averaged to  
202 obtain hourly measurements. The median floc size ( $D_{50}$ ) was obtained from  
203 the entire distribution as a single representative value of the floc size. Wa-  
204 ter samples during days 12-13 February 2008 were taken each hour from a  
205 CTD rosette for filtration on pre-weighted 0.4  $\mu m$  mesh size filters. Filters  
206 were weighted again to obtain mass concentration from the weight difference  
207 before and after filtration and from water sample volume. A linear relation-  
208 ship between these mass concentrations and corresponding LISST volume  
209 concentrations enabled to find a calibration formulation to convert the entire  
210 LISST recordings to mass concentrations (Ramírez-Mendoza et al., 2014).

211 The ADV employs the Doppler effect due to suspended particles to cal-  
212 culate the flow velocity (SonTek, 2002). The instrument recorded current ve-  
213 locity and pressure at 16 Hz during 20-minutes each hour at the same times  
214 as the LISST allowing simultaneous measurements of both instruments. The  
215 noise in ADV data was removed using a despiking algorithm based on a  
216 three dimensional phase space method by Mori et al. (2007) which is based  
217 on the method by Goring and Nikora (2002). We apply time-averaging of  
218 the 20 minute sampling period in order to obtain hourly values of turbu-  
219 lence statistics. Note that in the present investigation we are assuming a  
220 logarithmic velocity profile and both instruments LISST and ADV are in the  
221 approximately constant stress layer (Tennekes and Lumley, 1972).

222 *3.2. Hydrodynamic features from ADV*

223 Data measured by ADV are commonly used to extract information on  
 224 near-bed turbulence following Reynolds decomposition of the velocity com-  
 225 ponents. In the present study, we use the following decomposition to define  
 226 velocity fluctuations:

$$u' = U - \bar{u} \quad v' = V - \bar{v} \quad w' = W - \bar{w} \quad (1)$$

227 where  $U, V, W$  are the three components of the instantaneous velocity,  
 228 and  $\bar{u}, \bar{v}, \bar{w}$  the three components of the mean (time-averaged) velocity. Shear  
 229 stresses are then obtained using the covariances between fluctuations:

$$\tau_{cov} = \rho \sqrt{\overline{u'w'^2} + \overline{v'w'^2}} \quad (2)$$

230 where  $\rho$  is water density. Shear stresses using equations 1 and 2 were  
 231 obtained for the entire observation set from the ADV (with 20 minutes av-  
 232 eraging). The energy from fluctuations in equation 1 is given by:

$$K = \frac{1}{2}(\overline{u'^2} + \overline{v'^2} + \overline{w'^2}) \quad (3)$$

233 which we refer to as effective kinetic energy. It is critical to note here that  
 234 both the covariance stress  $\tau_{cov}$  and the effective kinetic energy  $K$  include fluc-  
 235 tuations that arise from both waves and turbulence. Many studies involving  
 236 both turbulence and waves in coastal environments decompose into a wave  
 237 contribution and a turbulence contribution instead (e.g. Trowbridge, 1998;  
 238 Bricker and Monismith, 2007; Feddersen, 2012). Even though the overlap  
 239 in the spatio-temporal scales affected by waves and turbulence, as well as  
 240 potential wave-turbulence interactions, complicate such decomposition, sev-  
 241 eral methods exist (e.g. Trowbridge, 1998; Bricker and Monismith, 2007).

242 However, in our case we focus on the effect of the fluctuations of fluid motion  
 243 on sediment flocs. From the point of view of the floc (particle) mechanics,  
 244 all fluid fluctuations act as an external force on the flocs, irrespective of their  
 245 provenance whether wave-induced or turbulence-induced. It is therefore im-  
 246 portant here to use quantities that measure the full combined effect of all  
 247 (wave and turbulence) fluctuations, as the covariance stress and the effective  
 248 kinetic energy respectively defined in equations 2 and 3.

249 An analysis was made to the entire dataset in order to compare the indi-  
 250 vidual effect of shear stress from currents and waves on sediment dynamics.  
 251 Provided that wave characteristics are known, shear stress from waves and  
 252 currents can be obtained following the spectral wave-current model of Mad-  
 253 sen (1994). Wave height ( $H_s$ ) and wave direction were obtained with the  
 254 PUV method. This method calculates surface spectra  $S_{\eta p}$  and  $S_{\eta u}$  using  
 255 pressure and velocity spectra  $S_p$  and  $S_u$ :

$$S_{\eta p} = \left( \frac{\cosh kh}{\cosh k(h+z)} \right)^2 \frac{S_p}{\rho_w^2 g^2} \quad (4)$$

$$S_{\eta u} = \left( \frac{\sinh kh}{\cosh k(h+z)} \right)^2 \frac{S_u}{\omega^2} \quad (5)$$

257 where  $k$  is wave number,  $h$  is mean water level relative to the seabed,  
 258  $z$  is vertical distance relative to the mean water level,  $\omega$  is wave angular  
 259 frequency (defined as  $2\pi f$ , where  $f$  is frequency in cycles per second),  $\rho_w$  is  
 260 water density and  $g$  is gravity. The value of  $k$  is calculated using the iterative  
 261 Newton-Raphson method given by Wiberg and Sherwood (2008) in the wave  
 262 dispersion relation:

$$\omega = \sqrt{gk \tanh kh} + kU_m \cos \alpha \quad (6)$$

263 where the second term on the right hand side is a modification to account  
 264 for the presence of a mean current  $U_m(=\sqrt{\bar{u}^2 + \bar{v}^2})$  with an angle  $\alpha$  with the  
 265 waves (Bolaños and Souza, 2010). The wave direction  $D_w$  is obtained using:

$$D_w = \arctan 2(S_{pu}, S_{pv}) \quad (7)$$

266 where  $\arctan 2$  is fourth quadrant arctangent of the real parts of the cross-  
 267 spectra between pressure-east velocity component ( $S_{pu}$ ) and pressure-north  
 268 velocity component ( $S_{pv}$ ). Spectral energy integration was used to calculate  
 269 the zeroth moment  $M_o$  and obtain the significant wave height ( $H_s$ ) as:

$$H_s = 4\sqrt{M_o} \quad (8)$$

270 The peak period ( $T_p$ ) is taken as the period with highest energy in the  
 271 wave spectra. Wave orbital velocities can be obtained following the linear  
 272 approach:

$$U_o = \frac{a_w \omega}{\sinh kh} \quad (9)$$

273 where  $a_w$  is wave amplitude ( $H_s/2$ ). Madsen (1994) assumes simple pe-  
 274 riodic plane waves and proposes an iterative method to calculate friction  
 275 velocities where the concept of wave friction factor is used. Thus:

$$\tau_w = \rho u_{*w}^2 \quad (10)$$

276

$$\tau_c = \rho u_{*c}^2 \quad (11)$$

277

$$\tau_{cw} = \rho u_{*cw}^2 \quad (12)$$

278 where  $\tau$  is shear stress,  $\rho$  is fluid density, the \* symbol denotes friction  
 279 velocity, subscripts  $w$ ,  $c$ ,  $cw$  are for waves, currents and combined waves and  
 280 currents, respectively.

281 Dissipation of turbulent kinetic energy  $\epsilon$  is estimated following the inertial  
 282 dissipation method. This method assumes that radian wavenumbers  $k_r$  at  
 283 which turbulence is produced are well separated from radian wavenumbers  
 284 at which turbulent kinetic energy is dissipated by viscosity and this range is  
 285 called the inertial range, where the flux of energy from high to low  $k_r$  must be  
 286 equal to the dissipation range if no sources or sinks of turbulent kinetic energy  
 287 are present (Huntley, 1988; Souza et al., 2011). Following Tennekes and  
 288 Lumley (1972) and Voulgaris and Trowbridge (1998), the turbulent spectrum  
 289 of the horizontal velocity component  $E_u(k_r)$  is:

$$E_u(k_r) = \frac{9}{55} \alpha \epsilon^{2/3} k_r^{-5/3} \quad (13)$$

290 and the turbulent spectrum for the vertical velocity used in this study  
 291  $E_w$  is obtained as:

$$E_w(k_r) = \frac{4}{3} E_u(k_r) \quad (14)$$

292 where  $\alpha=1.5$  is the Kolmogorov constant. The spectra obtained from  
 293 current velocities needs to be expressed as radian wavenumber  $k_r$  where the  
 294 Taylor hypothesis or also called frozen turbulence concept is applied. Surface  
 295 gravity waves could coincide with part of the inertial subrange. However, for  
 296 this study, there was no overlap between waves and the turbulent inertial  
 297 subrange. Once  $\epsilon$  is known, the Kolmogorov microscale of turbulence ( $\lambda$ )  
 298 and the turbulent shear parameter ( $G$ ) were obtained following:

$$\lambda = \left( \frac{\nu^3}{\epsilon} \right)^{1/4} \quad (15)$$

$$G = \left( \frac{\epsilon}{\nu} \right)^{1/2} \quad (16)$$

300 where  $\nu$  is kinematic viscosity.

## 301 4. Results

302 The analysis of the observations was divided in three regimes each five  
303 days long (Figs. 2 and 3). The first part occurs during neap tides (15  
304 February to 20 February), wave heights are very small ( $<0.1$  m), and the  
305 bottom current speed reaches up to  $0.28 \text{ m}\cdot\text{s}^{-1}$ . The ratio of current shear  
306 stress over wave shear stress,  $\tau_c/\tau_w$ , is the largest of the entire study with  
307 SPM concentration below  $50 \text{ mg}\cdot\text{l}^{-1}$ , and this part is therefore considered  
308 as a “**current-dominant**” regime. The second part occurs during spring  
309 tides (21 February to 26 February), bottom current speed reaches up to  $0.5$   
310  $\text{m}\cdot\text{s}^{-1}$ , and wave heights of  $0.5$  to  $1.4$  m are observed. The  $\tau_c/\tau_w$  ratio is  
311 significantly lower than during the previous regime, and this second part is  
312 defined as a combined “**currents-waves**” regime. During this regime was  
313 obtained the highest SPM concentration with  $350 \text{ mg}\cdot\text{l}^{-1}$ . The third and  
314 last part occurs again during neap tides (28 February to 05 March), bottom  
315 current speed is lower than for the first regime (less than  $0.2 \text{ m}\cdot\text{s}^{-1}$ ), and  
316 waves are the highest of the entire record with nearly  $2$  m height reached.  
317 The  $\tau_c/\tau_w$  ratio is the lowest of the study, and this regime is considered to  
318 be “**wave-dominant**”. Maxima of SPM concentration coincided with the  
319 highest wave heights and concentration of about  $150 \text{ mg}\cdot\text{l}^{-1}$ .

### 320 4.1. The flocc size spectrum

321 Flocc sizes measured by the LISST are shown for the three regimes in  
322 figure 4 with volume concentrations converted to mass concentrations. Since  
323 observations were taken during winter we assume the effect of organic mate-  
324 rial was minimal as has been found by some authors (e.g. Le Hir et al., 2007;

325 Fettweis et al., 2014) and in the Dee estuary by Todd (2014). An important  
326 feature of the floc size observations is the presence of one concentration peak  
327 at any time. This means the floc distribution is unimodal and the use of  $D_{50}$   
328 is a reasonable approximation. During the first regime (Fig. 4a), high con-  
329 centrations of small flocs coincided with flood and ebb phases while the high  
330 concentrations of large flocs happened with depth maxima and minima (close  
331 to slack water in the Dee). Concentrations diminished through the neap tide  
332 period but increased with tides at the end of the record. The “currents-  
333 waves” regime (Fig. 4b) presented the highest concentrations of both small  
334 and large flocs. Floc behaviour was similar as in the “current-dominant”  
335 case but amplified due to the hydrodynamic conditions and flocs reached the  
336 smallest size during this period. In the “wave-dominant” regime, concentra-  
337 tions were generally similar to the “current dominant” regime but lower than  
338 the “currents-waves” regime, except for two maxima on 1st March, and the  
339 relationship between floc size and tidal forcing is not as regular as in previous  
340 cases.

341 As expected, the behaviour of the flocs seems to be the result of turbulence-  
342 induced flocculation. Even though mass SPM concentration increases during  
343 resuspension events, there is no evidence of floc aggregation may be due to  
344 low SPM concentrations. Overall, the measured range of small and large flocs  
345 were  $\sim 50\text{-}100\mu\text{m}$  and  $\sim 300\text{-}350\mu\text{m}$ , respectively. During strong currents on  
346 flood and ebb, flocs in suspension are subjected to strong shear stresses and  
347 inter-particle collisions which result in break-up of large flocs and the mea-  
348 surement of high concentrations of small flocs. When shear stresses diminish  
349 around slack water, small flocs in suspension aggregate to form large flocs

350 and lead to diminish the concentration of small flocs and increase concen-  
351 tration of large flocs. Overall, from neap to spring tides there is an increase  
352 of shear stresses resulting in higher floc resuspension and break-up leading  
353 to the smallest floc sizes in flood and ebb of spring tides. The higher con-  
354 centration of small flocs leads to aggregation enhancement and bigger flocs  
355 during slack waters. The relative concentrations of small and large flocs are  
356 therefore determined by the turbulence magnitude, which is influenced by  
357 the presence of currents and waves. The mild conditions during the first  
358 regime were overwhelmed by the combination of both waves and currents in  
359 the second regime and the waves had the most important effect during the  
360 third regime with concentration maxima coinciding with the highest wave  
361 height.

#### 362 *4.2. Separated effect of currents and waves on flocculation*

363 Time series of shear stress from waves  $\tau_w$  and currents  $\tau_c$  are presented in  
364 figure 5 along with median floc size  $D_{50}$  for the three hydrodynamic regimes.  
365 The “current-dominant” regime (Fig 5a) confirms that shear stress from  
366 waves was negligible in comparison with stress from currents. This regime  
367 showed an increase in shear stress magnitude from about 0.10 Pa to 0.35 Pa  
368 towards the spring tide which means more energetic conditions and thus floc  
369 break-up. This is consistent with the general trend for the floc size following  
370 which the intra-tidal minimum floc size diminished from 70  $\mu m$  to 60  $\mu m$  and  
371 the intra-tidal maximum floc size diminished from 240  $\mu m$  to 160  $\mu m$ , both  
372 over the duration of this regime. There was a clear quarter-diurnal variability  
373 for the shear stress with flood-ebb asymmetry showing higher values during  
374 ebb than during flood. This asymmetry resulted in stronger floc disaggrega-

375 tion during the ebbs, and ebb flocs smaller than flood flocs. Minimum values  
376 of shear stress also presented differences with effects on floc sizes. Shear  
377 stress minima after ebb phase had considerably lower values than after flood  
378 and this allowed floc growth resulting in smallest flocs during slack waters  
379 after ebb.

380 For the “currents-waves” regime (Fig 5b), shear stress from waves had the  
381 same order of magnitude as shear stress from currents, in particular during  
382 the first two days. Both stresses reached in excess of 0.75 Pa on 22 February.  
383 Wave stress was tidally modulated and in phase with current stress with  
384 the same quarter-diurnal variability persistent throughout the entire period.  
385 This tidal modulation of waves has already been reported for the Dee estuary  
386 by Bolaños et al. (2014). From the processes causing a wave tidal modulation  
387 mentioned by Davidson et al. (2009), the current-wave interaction itself is  
388 maybe the main factor happening in the study site. The combination of  
389 stress from waves and currents resulted in the smallest flocs ( $50 \mu m$ ) of the  
390 three regimes, while the largest flocs barely reached  $150 \mu m$ , in particular  
391 during the first two days when waves were the largest for this regime. During  
392 the last two days, wave stress diminished and floc size behaviour became  
393 qualitatively identical to that of the “current-dominant” regime although the  
394 size of the small flocs remained in  $50 \mu m$  due to spring tide hydrodynamic  
395 forcing. The resulting floc size variability was the highest of the three regimes,  
396 with a range of 50-225  $\mu m$ . The quarter-diurnal behaviour was similar to  
397 that of the previous regime with weaker shear stress during flood than ebb.  
398 However,  $D_{50}$  minima were of similar magnitude ( $\sim 50 \mu m$ ) although slightly  
399 diminished to the end of record when shear stress from waves was half the

400 magnitude of the stress of currents. During slack waters in this regime large  
401 flocs were present as in the “current-dominant” regime, with the largest flocs  
402 after ebb phase and an important difference with floc size after flood that  
403 reached  $100 \mu m$  on 23 February.

404 The “wave-dominant” regime is shown in figure 5c where shear stress from  
405 waves reached more than 2 Pa, and those from currents remained about  
406 0.5 Pa as in previous regimes. In this regime, wave shear stresses almost  
407 lost the neap-spring tidal modulation and also the quarter-diurnal variability  
408 found in the combined regime. The highest wave shear stresses were present  
409 during three consecutive days (1-3 March). These maxima coincided with  
410 the smallest median floc sizes of about  $60 \mu m$  in this regime. These periods  
411 were followed by calm conditions and an increase in  $D_{50}$  values of more than  
412  $180 \mu m$ . Floc behaviour during this regime was therefore the response only  
413 to wave conditions and also the highest shear stresses were present during  
414 this regime. Nevertheless, these not resulted in the smallest median floc sizes  
415 and instead showed the lowest  $D_{50}$  variability of the three regimes which may  
416 represent an equilibrium between floc break-up and aggregation around  $60$   
417  $\mu m$ .

418 In summary: (i) the “current-dominant” regime had the highest floc size  
419 variability with clear floc aggregation and break-up, (ii) with the “currents-  
420 waves” combined effect floc break-up became dominant and aggregation di-  
421 minished, and (iii) when shear stress from waves is more important seems  
422 to be a balance of aggregation and break-up processes. Therefore, the effect  
423 of generated turbulence from currents and waves on the flocculation pro-  
424 cess seemed to affect at different magnitudes and maybe in different ways.

425 However, the specific behaviour of the flocs in response to the turbulence  
426 conditions from the three different regimes is still unknown. In addition,  
427  $D_{50}$  asymmetries between flood and ebb phases appeared to reflect effects of  
428 turbulence which depends on flow direction. The next section analyses the  
429 relationships of the median floc size and turbulent properties important for  
430 the flocculation process.

### 431 *4.3. Flocculation controls*

432 Relationships between median floc size and shear stress, effective kinetic  
433 energy and dissipation rate are shown in figure 6 for the entire dataset cover-  
434 ing all three regimes. Shear stresses using the covariance (Eq. 2) and spectral  
435 (Eq. 12) methods are shown in figures 6a and 6b, respectively. Both shear  
436 stresses presented an inverse relationship with median floc size, although  $\tau_{cov}$   
437 had higher values and  $\tau_{cw}$  presented a slightly different data distribution,  
438 with a small amount of data corresponding to large flocs and about  $1 \times 10^{-2}$   
439 Pa while small flocs presented a wider distribution.

440 The relationship between  $D_{50}$  and  $K$  also showed an inverse relationship  
441 in a clearly defined population (Fig. 6c). Dissipation (Fig. 6d) has been  
442 included because it is used to calculate shear rate  $G$  and the Kolmogorov  
443 microscale of turbulence  $\lambda$ . This showed two populations, one with similar  
444 inverse relationship as the other variables and a second population for dissi-  
445 pation approximately constant. From all the relationships, floc size with  $\tau_{cov}$   
446 and  $K$  had the simplest distributions since only one population of data can  
447 be distinguished. Furthermore, a lower scatter of points is obtained when  
448 relating  $D_{50}$  to  $K$ , which would result in a decrease in the uncertainty when  
449 a curve fitting is applied to the data ( $R^2$  value using  $\tau_{cov}$  is 0.48 while using

450  $K$  is 0.58). Even though the variability of median floc size remains high for  
451 a given value of effective kinetic energy, this range of floc sizes is smaller  
452 than for any of the other variables  $\tau_{cov}$ ,  $\tau_{cw}$  and  $\epsilon$ . These results suggest  
453 that  $K$  may give better approximations if used to describe floc size changes.  
454 To further analyse this hypothesis, values of  $\tau_{cov}$  and  $K$  were divided in hy-  
455 drodynamic regimes and flood and ebb phases. In addition, to observe the  
456 effects of the dissipation rate on other variables, the same analysis is carried  
457 out for the Kolmogorov microscale and shear parameter.

#### 458 4.4. Shear stress and effective kinetic energy

459 Observations relating  $D_{50}$  and  $\tau_{cov}$  are shown in figure 7 in panels a, c, and  
460 e for “current-dominant”, “currents-waves” and “wave-dominant” regimes,  
461 respectively, and flood and ebb phases. The range of  $\tau_{cov}$  values is slightly  
462 different for each regime. As expected, highest  $\tau_{cov}$  values were obtained  
463 during the “currents-waves” regime while the lowest during the “current-  
464 dominant” regime. In contrast, the “wave-dominant” case showed the lowest  
465 variability of shear stress. Floc sizes mainly differ in minimum values. The  
466 smallest flocs during the “current-dominant” and “wave-dominant” regimes  
467 were of about  $60 \mu m$  diameter, while the smallest flocs in the “currents-  
468 waves” regime were about  $40 \mu m$  according to the highest values of  $\tau_{cov}$  for  
469 this case. The most important feature is that the relationship follows the  
470 same pattern during flood and ebb phases. These phases show only a shift  
471 but the distribution remains the same and the magnitude of the shift seems  
472 to be similar for the three regimes. Unlike the “current-dominant” regime,  
473 “currents-waves” and “wave-dominant” regimes present a wide scatter of  
474 data.

475 Figure 7 in panels b, d and f shows the relationship during the three  
476 regimes and flood and ebb tidal phases between  $K$  and  $D_{50}$ . All regimes  
477 showed the same behaviour, like in the case of  $\tau_{cov}$ , an inverse relationship  
478 with differences in magnitudes and tidal phases. The “current-dominant”  
479 and “currents-waves” regimes were characterised by higher energy during ebb  
480 phases. This intratidal difference in effective kinetic energy magnitude means  
481 the shift previously found is also present in these two regimes for the energy  
482 variable although smaller than the shift for the  $\tau_{cov}$  case. The difference be-  
483 tween flood and ebb is almost undistinguishable during the “wave-dominant”  
484 regime (Fig. 7f).

485 Results of the relationships between median floc size, shear stress and  
486 effective kinetic energy demonstrate the possibility to describe the floc be-  
487 haviour with simple formulations derived from the log-log plots of the vari-  
488 ables. Moreover, better quantitative results should be obtained if flood and  
489 ebb tidal phases are also taken into account.

#### 490 4.5. Turbulent shear parameter and Kolmogorov microscale

491 Another commonly used property to assess the turbulence effect on the  
492 flocculation process is the shear parameter  $G$ , shown in figure 8 (panels a,  
493 c and e), which is a measure of the turbulent shear rate in the flow and  
494 therefore strongly related to floc sizes. Despite the wide scatter of data, two  
495 populations can be distinguished in figures 8a and 8c. A large population  
496 during ebb phase with, as expected, an inverse relationship shows small flocs  
497 for high shear rate and increasing sizes with decreasing shear rate. A second  
498 small population appears almost in the middle of the aforementioned popu-  
499 lation during flood and is characterised by approximately constant  $G$  values.

500 However, a random behaviour is also noticeable when floc size increases above  
501  $100 \mu m$ . This is also present during the ebb phase in the “current-dominant”  
502 regime. The “wave-dominant” regime is characterised by a wide spread of  
503 data without any important difference between flood and ebb phases or dif-  
504 ferent populations (Fig. 8e). Differences between the three regimes and flood  
505 and ebb tidal phases are present but there is no single relationship for all the  
506 cases.

507 The smallest eddies in the turbulent flow are represented by the Kol-  
508 mogorov microscale  $\lambda$ , which is assumed to be a floc size threshold (e.g.  
509 Winterwerp and van Kesteren, 2004). Results for this study are shown in  
510 figure 8 panels b, d and f for the three regimes. Data show two clear dif-  
511 ferent populations when flocs are smaller than  $200 \mu m$  with a similar data  
512 scattering as for the shear rate  $G$ . One of these populations is further iden-  
513 tified as occurring during flood for the “current-dominant” (Fig. 8b) and  
514 “currents-waves” (Fig. 8d) regimes with low variability of  $\lambda$  values. No clear  
515 behaviour was found for floc sizes larger than  $200 \mu m$  in any tidal phase of  
516 the “current-dominant” regime while for the ebb phase in “currents-waves”  
517 regime a direct relationship was present for all floc sizes. A different case was  
518 shown for the “wave-dominant” regime when the differences between tidal  
519 phases were not as clear as in previous cases although a direct relationship  
520 is present with a wide data scattering (Fig. 8f).

## 521 **5. Discussion**

522 The “current dominant” regime is probably the simplest of the three  
523 regimes and the one where the flocculation response to turbulent conditions

524 is most evident. In general, the floc sizes are larger during neap tides than  
525 during spring tides as a result of weaker turbulent conditions (Fig. 5a). Low  
526 turbulence allows floc aggregation while break-up is not enough strong during  
527 neaps. These conditions change during spring tides and break-up becomes  
528 important. There is also interesting behaviour of the floc size variability  
529 at the semidiurnal frequency. Shear stress minima after ebb phase falls to  
530 nearly zero values coinciding with large flocs (see for example figure 5a at  
531 the end of day 15) while after flood stress is not as low and flocs are not as  
532 large as after ebb (see figure 5a on day 16 after the first grey bar). Large  
533 flocs at low water could be the result of aggregation of small flocs due to  
534 turbulent motions and either locally resuspended, or advected from upper  
535 parts of the estuary during the long ebb phase since advection of suspended  
536 sediments is an important process in the Dee Estuary under such calm neap  
537 tide conditions (Amoudry et al., 2014). Asymmetries in shear stress maxima  
538 coincide with asymmetries in floc size minima as a direct result of turbulence  
539 magnitude. For example, in figure 5a on the first half of day 17 the maxima  
540 stresses were  $\sim 0.08$  Pa for flood and  $\sim 0.14$  Pa for ebb with floc sizes of  $\sim 100$   
541  $\mu m$  and  $\sim 90$   $\mu m$ , respectively (ellipses in fig. 5a).

542 The “currents-waves” regime is characterized by an enhancement of the  
543 conditions of the “current dominant” case, with higher concentrations of  
544 smaller and larger flocs for high and low energy conditions, respectively. The  
545 combined effect of currents and waves shear stresses first resuspends small  
546 flocs from the bed to upper parts of the water column, then resuspends large  
547 flocs which are subsequently disaggregated and thus measured as small flocs.  
548 Other possibility is that particles are firstly resuspended from the bottom,

549 then aggregate and formed flocs adjust to the present turbulent conditions.  
550 Since waves are tidally modulated (Bolaños et al., 2014), the decrease in  
551 shear stress from waves and currents is likely to occur at nearly the same  
552 time and enhances the aggregation of suspended flocs which are measured as  
553 large flocs in also high concentrations.

554 Shear stress during the “wave-dominant” regime was the highest of the  
555 entire record and therefore the highest erosion, resuspension and disaggre-  
556 gation were expected. However, concentrations are lower and flocs are not  
557 as small as during the “currents-waves” regime. It is possible that in the  
558 “currents-waves” case high concentrations are present at low levels while  
559 in the “wave-dominant” case with higher energy conditions suspended sedi-  
560 ments could be dispersed over the entire water column and thus not recorded  
561 by measurements at a given level. Bartholomä et al. (2009) measured sus-  
562 pended sediments through the water column in higher concentrations during  
563 high waves conditions than during calm periods and modelling results by  
564 Stanev et al. (2006) also showed this behaviour. Even though the “currents-  
565 waves” is the regime with extreme floc sizes, a more important comparison  
566 is between the “current dominant” and “wave-dominant” regimes as these  
567 occurred during similar tidal conditions. Floc behaviour in response to tidal  
568 currents is almost completely overwhelmed by the presence of waves, which  
569 are only slightly affected by tidal modulation.

570 Floc size changes seem to be also related to their distribution in the  
571 water column. As mentioned before, the flocculation process is enhanced  
572 during the “currents-waves” regime. However, the “wave-dominant” regime  
573 is characterised by longer periods of sustained high shear stress. In these

574 conditions flocs at the seabed are taken into suspension and a possible “steady  
575 state” could be achieved near the bottom as described by Puls et al. (1988).  
576 According to the authors, a “steady state” may occur if flocs in higher parts  
577 of the water column, away from the bottom but far enough from the surface,  
578 are subjected to less turbulent conditions and therefore aggregate to bigger  
579 flocs which then fall to high energy lower parts where they disaggregate  
580 and are again raised to higher parts. This could explain the floc size low  
581 variability during the higher energy events of the “wave-dominant” regime.  
582 A second possible explanation is that a longer effect of shear stress causes  
583 the erosion of flocs in the process of consolidation on the sea bed but is not  
584 enough to break them and therefore remain slightly larger than the firstly  
585 resuspended weak flocs. There is also another possibility for the floc size low  
586 variability during this regime and is that flocs aggregate to a certain size and  
587 cannot continue growing because of the sustained agitation by both waves  
588 and turbulence. At the end of this regime the floc size range increase, 100-240  
589  $\mu m$ , and this is likely due to the flocs left in suspension by the effect of waves.  
590 The wave shear stress decrease during the last one and a half days allowing  
591 for the currents shear stress to be the dominant effect with the semidiurnal  
592 variability, but with a higher floc size range. A decrease in this range and  
593 similar behaviour to the “current dominant” regime are expected if no more  
594 waves are present.

### 595 5.1. $D_{50}$ relationships with $\tau_{cov}$ and $K$

596 Data scattering for all hydrodynamic regimes and all tidal phases seems  
597 to be lower in the relationship of  $D_{50}$  with  $K$  than with  $\tau_{cov}$  as shown in  
598 figure 7. This suggested the possibility to describe floc size changes using

599 simple equations of a power of the effective kinetic energy of the form:  $D_{50} =$   
 600  $A \cdot (K)^B$ . Using this form, a test was carried out adjusting curves to the  
 601 data distributions of figure 7. The resulting coefficients of determination  
 602  $R^2$ , are shown in table 5.1 in order to compare the use of  $K$  and  $\tau_{cov}$  for  
 603 the description of floc size, as well as how the regime and tidal separation  
 604 improves their relationship. Except for the flood phase during the “current  
 605 only” regime, the use of effective kinetic energy produces the best fits to the  
 606 data according to  $R^2$  values. Improvements from 2% (“current dominant”-  
 607 ebb) to 26% (“wave-dominant”-ebb) and of 30% for the “wave-dominant”  
 608 regime and both phases are reached using  $K$ . The minimum  $R^2$  difference  
 609 is obtained in the “current dominant” regime, it increases in the combined  
 610 regime and is maximum in the “wave-dominant” regime, which emphasizes  
 611 the important role of the waves in the process. Therefore, a better floc  
 612 size predictor seems to be the effective kinetic energy instead of the widely  
 613 used turbulent stress or turbulent shear rate (e.g. Winterwerp et al., 2006;  
 614 Manning et al., 2010; Kombiadou and Krestenitis, 2012). This also seems to  
 615 be particularly true in the presence of waves.

## 616 5.2. $D_{50}$ relationships with $G$ and $\lambda$

617 The relationships between floc size  $D_{50}$  and the turbulent shear parameter  
 618  $G$  follow the behaviour reported by different authors during ebb and part of  
 619 the flood (e.g. Mietta et al., 2011; Verney et al., 2011; Wang et al., 2013), i.e.  
 620 low shear rate corresponds to larger flocs and their size decrease as shear rate  
 621 increase. The high scatter floc behaviour for the “current-dominant” regime  
 622 at low  $G$  values has also been found in other studies (Winterwerp, 1998;  
 623 Verney et al., 2011). The “currents-waves” regime during ebb has a clear

624 aggregation and disaggregation behaviour. Higher data scattering was found  
625 during the “wave-dominant” case on both flood and ebb phases. Turbulent  
626 shear rate seems to have the expected effect during ebb phases. Floccs in  
627 the present study were smaller than the Kolmogorov microscale which is  
628 in agreement with different studies (e.g. Braithwaite et al., 2012; Fettweis  
629 et al., 2006; Cross et al., 2013; Son and Hsu, 2011), larger floccs than  $\lambda$  have  
630 also been reported (e.g. Cross et al., 2013). In addition, floccs cannot reach  
631 the Kolmogorov microscale on either hydrodynamic regime or tidal phase.  
632 The specific behaviour of the Kolmogorov microscale is similar to the shear  
633 parameter, increase in  $\lambda$  coincides with increase in median flocc size for ebb  
634 and part of the flood phases when floccs were higher than  $200 \mu m$ .

635 The Kolmogorov microscale relationship with  $D_{90}$  flocc size is shown in  
636 figure 9 for comparison with  $\lambda - D_{50}$  relationship in figure 8. Overall,  $D_{90}$   
637 values are about  $150 \mu m$  higher than  $D_{50}$  with similar time series behaviour  
638 (data not shown) as has also been found experimentally by Verney et al.  
639 (2011). The use of  $D_{90}$  led the flocc sizes around the Kolmogorov microscale  
640 with good correlation for the ebb phase in all the regimes. However, slightly  
641 larger values in the case of the “current-dominant” regime can be seen and  
642 also some values were higher than the instrument upper limit. This is not  
643 as clear during the other two regimes. Flood phases still presented the same  
644 behaviour as for the  $D_{50}$  case.

645 The difference between flood and ebb behaviour of  $G$  and  $\lambda$  is related  
646 with asymmetries in turbulent dissipation. These asymmetries are shown in  
647 figure 10 with the expected semidiurnal variability. Overall, during ebb phase  
648 dissipation values were higher than during flood with differences of about one

649 order of magnitude. In particular, dissipation variability during flood phases  
650 is lower than during ebb. Extreme minima values are also observed at low  
651 slack waters mainly during the first two regimes which correspond with some  
652 of the randomly results at large floc sizes in figure 8a to 8d and occur when  
653 turbulence is maybe too low for the dissipation calculations be valid.

### 654 *5.3. Flood and ebb tidal phases*

655 The scatter of data still present when observations are divided into flood  
656 and ebb phases may be due to the hysteresis effect. This is one of the most im-  
657 portant and scarcely mentioned features of the cohesive sediment behaviour  
658 and its effect can be seen in the relationship of a number of different variables:  
659 turbulent stresses, SPM concentration, current speed, Reynolds stresses, tur-  
660 bulent kinetic energy and median floc size (e.g. Dyer, 1986; Fettweis et al.,  
661 2012; Wang et al., 2013). It has been stated that this effect is due to a time  
662 lag in the response between different variables (e.g. Verney et al., 2011).  
663 The floc size behaviour during flood and ebb periods in the present study  
664 is similar to results in the Belgian coast presented by Fettweis et al. (2012).  
665 The authors showed periods of neap tides without the effect of waves with  
666 clear difference between the flood and ebb periods as in the “current only”  
667 and “currents-waves” regimes, while during storms the observations showed  
668 high scatter with a slight difference between tidal phases as in the “wave-  
669 dominant” case.

670 Figure 11 shows an example of the hysteresis effect during a tidal cycle  
671 of the present investigation. The flood phase starts at low energy conditions  
672 (red triangle). The floc size diminishes as the energy increases until the  
673 system reaches maximum energy and a minimum median floc size. When

674 the energy decreases, the floc size increases with values slightly greater until  
675 the phase finishes (red circle). The behaviour during the ebb phase (in blue)  
676 is similar in floc size changes but with a shift in the values of turbulent  
677 kinetic energy. This particular feature seems to add another variable to  
678 the flocculation process since the size of the flocs at the end of one phase is  
679 important for the beginning of the next phase, i.e., the effect of the turbulence  
680 will be different on flocs of slightly different sizes and also small changes in  
681 turbulence will have a different effect. In summary, the first characteristic  
682 of the behaviour of the floc size with respect to turbulent properties is their  
683 inverse relationship, the second feature is the shift between tidal phases and  
684 the third is the hysteresis phenomenon. The last two characteristics may  
685 explain part of the important scattering in the observations during the same  
686 tidal phase.

## 687 **6. Conclusions**

688 In the present investigation the response of the flocculation process due to  
689 turbulence from different hydrodynamic conditions and intra-tidal variability  
690 was investigated. To achieve this, field observations were used to characterise  
691 floc size behaviour in a hypertidal estuary. Three hydrodynamic regimes were  
692 defined based on the magnitude of the effect of currents and waves.

693 During the “currents-dominant” regime currents were the main forcing  
694 factor and typical floc aggregation and break-up was found with low and  
695 high energy conditions, respectively. The presence of waves in the “currents-  
696 waves” regime coincided with strong currents in spring tides enhancing the  
697 turbulence-induced flocculation process. Floc sizes during this second regime

698 presented the highest variability of the entire study. High shear stress led to  
699 the smallest flocs while low shear stress to a wide range of large flocs because  
700 of break-up and aggregation, respectively. During the “wave-dominant”  
701 regime waves were the most important forcing factor and shear stresses  
702 reached their highest values. However, flocculation was significantly dimin-  
703 ished with floc sizes showing almost constant values coinciding with the high-  
704 est waves. This could be due to floc distribution along the water column or  
705 a possible floc steady state.

706 The relationships of floc size and shear stress and effective kinetic energy,  
707 showed the commonly found inverse relationship and high data scattering.  
708 In the case of effective kinetic energy, the scattering was lower suggesting  
709 a better predictor of floc size. Data separation in hydrodynamic regimes  
710 and flood-ebb phases also reduced significantly the data scattering with the  
711 intra-tidal variability characterised by a shift while still showing the inverse  
712 relationship. The only exception was the “wave-dominant” regime. These  
713 results are confirmed when curve fittings were applied to these separated  
714 data resulting in improvements of the determination coefficients  $R^2$  of up to  
715 26%. Overall, determination coefficients of the separated distributions were  
716 better for effective kinetic energy than for shear stress.

717 The relationship between floc size and turbulent shear rate showed the ex-  
718 pected inverse relationship only during ebb phases while during flood changes  
719 in floc sizes happened with low variability of  $G$  values. Median floc size was  
720 lower than the Kolmogorov microscale of turbulence which is anticipated  
721 because of the winter season. During flood the Kolmogorov microscale pre-  
722 sented low variability. The low variability of both  $G$  and  $\lambda$  during flood was

723 related to current tidal asymmetries. These tidal differences seem to be en-  
724 hanced when dissipation values are calculated (Eq. 14) and in turn used to  
725 calculate the Kolmogorov microscale of turbulence and turbulent shear rate  
726 (Eqs. 15 and 16).

727 Results of this study showed hydrodynamic conditions are important for  
728 the floc size behaviour and part of the wide data scattering is explained by  
729 flood and ebb tidal phases with the hysteresis effect also playing an important  
730 role. Taking into account these features may lead to better results when  
731 proposing formulations to describe the flocculation process. In particular, the  
732 use of an effective kinetic energy instead of shear stresses in numerical models  
733 could result in improved predictions of flocculation when both currents and  
734 waves are present.

### 735 **Acknowledgements**

736 We want to acknowledge the organizations of the United Kingdom and  
737 México which provided the funding and opportunity for this investigation  
738 to be carried out: NERC (National Environmental Research Council via  
739 the iCOASST project, grant NE/J005444/1), NOC (National Oceanography  
740 Centre) and CONACyT (Consejo Nacional de Ciencia y Tecnología through  
741 the PhD Scholarship ID 212026), CICESE (Centro de Investigación Científica  
742 y de Educación Superior de Ensenada). We also want to thank Dr. Romaric  
743 Verney for his important comments to improve the study presented in this  
744 manuscript.

745 **References**

- 746 Agrawal, Y., Pottsmith, H., 2000. Instruments for particle size and settling  
747 velocity observations in sediment transport. *Marine Geology* 168, 89–114.
- 748 Amoudry, L. O., Ramírez-Mendoza, R., Souza, A. J., Brown, J. M., 2014.  
749 Modelling-based assessment of suspended sediment dynamics in a hyper-  
750 tidal estuarine channel. *Ocean Dynamics* 64, 707–722, doi:10.1007/s10236-  
751 014-0695-8.
- 752 Bartholomä, A., Kubicki, A., Badewien, T. H., Flemming, B. W., 2009.  
753 Suspended sediment transport in the German Wadden Sea—seasonal vari-  
754 ations and extreme events. *Ocean Dynamics* 59, 213–225.
- 755 Bass, S., Aldridge, J., McCave, I., Vincent, C., 2002. Phase rela-  
756 tionships between fine sediment suspensions and tidal currents in  
757 coastal seas. *Journal of Geophysical Research* 107 (C10), 10–1–10–14,  
758 doi:10.1029/2001JC001269.
- 759 Bolaños, R., Brown, J. M., Amoudry, L. O., Souza, A. J., 2013. Tidal, River-  
760 ine and Wind Influences on the Circulation of a Macrotidal Estuary. *Jour-  
761 nal of Physical Oceanography* 43, 29–50, doi: 10.1175/JPO-D-11-0156.1.
- 762 Bolaños, R., Brown, J. M., Souza, A. J., 2014. Wave-current interactions in  
763 a tide dominated estuary. *Continental Shelf Research* 87, 109–123, doi:  
764 10.1016/j.csr.2014.05.009.
- 765 Bolaños, R., Moate, B., Souza, A. J., 2009. Measuring suspended sediment  
766 and its wave and turbulence forcing in the dee estuary. In: Mizuguchi, M.,

- 767 Sato, S. (Eds.), Coastal Dynamics 2009: Impacts of human activities on  
768 dynamic coastal processes, Japan. World Scientific. Vol. 43. p. 12, paper  
769 119.
- 770 Bolaños, R., Souza, A. J., 2010. Measuring hydrodynamics and sediment  
771 transport processes in the Dee Estuary. *Earth System Science Data* 2,  
772 157–165.
- 773 Braithwaite, K., Bowers, D., Nimmo-Smith, W., Graham, G., 2012. Con-  
774 trols on flocculation in an energetic tidal channel. *Journal of Geophysical*  
775 *Research* 117, 1–12, doi:10.1029/2011JC007094.
- 776 Bricker, J., Monismith, S., 2007. Spectral wave-turbulence decomposi-  
777 tion. *Journal of Atmospheric and Oceanic Technology* 24 (8), 1479–1487,  
778 doi:10.1175/JTECH2066.1.
- 779 Brown, J. M., Bolaños, R., Souza, A. J., 2014. Process contribution to the  
780 time-varying residual circulation in tidally dominated estuarine environ-  
781 ments. *Estuaries and Coasts* 37, 1041–1057, DOI 10.1007/s12237-013-9745-  
782 6.
- 783 Camenen, B., 2009. Discussion of Uncertainty of excess density and  
784 settling velocity of mud derived from in situ measurements by M.  
785 Fettweis. *Estuarine Coastal & Shelf Science* 78(2), June 2008. doi:  
786 10.1016/j.ecss.2008.01.007. *Estuarine, Coastal and Shelf Science* 83, 111–  
787 112, doi:10.1016/j.ecss.2008.08.013.
- 788 Cross, J., Nimmo-Smith, W., Torres, R., Hosegood, P., 2013. Biological con-  
789 trols on resuspension and the relationship between particle size and the

- 790 kolmogorov length scale in a shallow coastal sea. *Marine Geology* 343,  
791 29–38.
- 792 Dankers, P., Winterwerp, J., 2007. Hindered settling of mud flocs:  
793 Theory and validation. *Continental Shelf Research* 27, 1893–1907,  
794 doi:10.1016/j.csr.2007.03.005.
- 795 Davidson, M., O’Hare, T., George, K., 2009. Tidal modulation of incident  
796 wave heights: Fact or Fiction? *Reef Journal* 1 (1), 16–32.
- 797 Davies, E., Nimmo-Smith, W., Agrawal, Y., Souza, A., 2012. Lisst  
798 100 response to large particles. *Marine Geology* 307-310, 117–122,  
799 doi:10.1016/j.margeo.2012.03.006.
- 800 Dyer, K. R., 1986. *Coastal and Estuarine Sediment Dynamics*. John Wiley  
801 & Sons, pp 342.
- 802 Dyer, K. R., 1989. Sediment processes in estuaries: future research require-  
803 ments. *Journal of Geophysical Research* 94 (C10), 14327–14339.
- 804 Feddersen, F., 2012. Observations of the surf-zone turbulent dissipation rate.  
805 *Journal of Physical Oceanography* 42 (3), 386–399.
- 806 Fettweis, M., Baeye, M., Lee, B., Chen, P., Yu, J., 2012. Hydro-  
807 meteorological influences and multimodal suspended particle size distri-  
808 butions in the belgian nearshore area (southern north sea). *Geo-Marine*  
809 *letters* 32, 123–137, dOI 10.1007/s00367-011-0266-7.
- 810 Fettweis, M., Baeye, M., Van der Zande, D., Van den Eynde, D., Lee, B.,

- 811 2014. Seasonality of flocculation strength in the southern North Sea. *Journal of*  
812 *Geophysical Research* 119, 1911–1926, doi:10.1002/2013JC009750.
- 813 Fettweis, M., Francken, F., Pison, V., Van den Eynde, D., 2006. Suspended  
814 particulate matter dynamics and aggregate sizes in a high turbidity area.  
815 *Marine Geology* 235, 63–74.
- 816 Fugate, D., Friedrichs, C., 2003. Controls on suspended aggregate size in  
817 partially mixed estuaries. *Estuarine, Coastal and Shelf Science* 58, 389–  
818 404.
- 819 Goring, D., Nikora, V., 2002. Despiking acoustic doppler velocimeter data.  
820 *Journal of Hydraulic Engineering* 128 (1), 117–126, 10.1061/(ASCE)0733-  
821 9429(2002)128:1(117).
- 822 Graham, G. W., Nimmo-Smith, A. M., 2010. The application of holography  
823 to the analysis of size and settling velocity of suspended cohesive sediments.  
824 *Limnology and Oceanography: Methods* 8, 1–15.
- 825 Halliwell, A., 1973. Residual drift near the sea bed in Liverpool Bay: an ob-  
826 servational study. *Geophysical Journal of the Royal Astronomical Society*  
827 32, 439–458.
- 828 Holden, V., Worsley, A., Booth, C., Lymer, G., 2011. Characterisation and  
829 sediment-source linkages of intertidal sediment of the UK's north Sefton  
830 coast using magnetic and textural properties: findings and limitations.  
831 *Ocean Dynamics* 61 (12), 2157–2179.
- 832 Huntley, D., 1988. A modified inertial dissipation method for estimating  
833 seabed stresses at low Reynolds numbers, with application to wave/current

- 834 boundary layer measurements. *Journal of Physical Oceanography* 18, 339–  
835 346.
- 836 Jago, C. F., Jones, S. E., 1998. Observation and modelling of the dynamics  
837 of benthic fluff resuspended from a sandy bed in the Southern North Sea.  
838 *Continental Shelf Research* 18 (11), 1255–1282.
- 839 Khelifa, A., Hill, P. S., 2006. Models for effective density and settling velocity  
840 of flocs. *Journal of Hydraulic Research* 44 (3), 390–401.
- 841 Kombiadou, K., Krestenitis, N. Y., 2012. Fine sediment transport model for  
842 river influenced microtidal shelf seas with application to the Thermaikos  
843 gulf. *Continental Shelf Research* 36, 41–62.
- 844 Krivtsov, V., Howarth, M. J., Jones, S. E., Souza, A. J., Jago, C. F., 2008.  
845 Monitoring and modelling of the Irish Sea and Liverpool Bay: An overview  
846 and SPM case study. *Ecological Modelling* 212, 37–52.
- 847 Le Hir, P., Monbet, Y., Orbain, F., 2007. Sediment erodability in sediment  
848 transport modelling: Can we account for biota effects? *Continental Shelf*  
849 *Research* 27, 1116–1142, doi:10.1016/j.csr.2005.11.016.
- 850 Madsen, O., 1994. Spectral wave-current bottom boundary layer flows. In:  
851 Edge, B. (Ed.), *Proceedings of the 24th International Conference on*  
852 *Coastal Engineering*. ASCE, pp. 384–398, Kobe, Japan.
- 853 Maerz, J., Verney, R., Wirtz, K., Feudel, U., 2011. Modeling flocculation  
854 processes: Intercomparison of a size class-based model and  
855 a distribution-based model. *Continental Shelf Research* 31, S84–S93,  
856 doi:10.1016/j.csr.2010.05.011.

- 857 Maggi, F., 2007. Variable fractal dimension: A major control for flocculation structure and flocculation kinematics of suspended cohesive sediment. *Journal of Geophysical Research* 112 (C07012), 1–12.
- 858  
859
- 860 Maggi, F., 2008. Stochastic flocculation of cohesive sediment: Analysis of flocculation mobility within the flocculation size spectrum. *Water Resources Research* 44 (WO1433), doi:10.1029/2007WR006109.
- 861  
862
- 863 Manning, A., Baugh, J., Spearman, J., Whitehouse, R., 2010. Flocculation settling characteristics of mud: sand mixtures. *Ocean Dynamics* 60, 237–253.
- 864  
865
- 866 Manning, A., Dyer, K., 1999. A laboratory examination of flocculation characteristics with regard to turbulent shearing. *Marine Geology* 160, 147–170.
- 867
- 868 Mehta, A., 1988. Laboratory studies on cohesive deposition and erosion. In: Dronkers, J., van Leussen, W. (Eds.), *Physical Processes in Estuaries*. Springer-Verlag, p. 560.
- 869  
870
- 871 Mietta, F., Chassagne, C., Verney, R., Winterwerp, J., 2011. On the behavior of mud flocculation size distribution: model calibration and model behavior. *Ocean Dynamics* 61, 257–271, doi:10.1007/s10236-010-0330-2.
- 872  
873
- 874 Mikkelsen, O. A., Hill, P., Milligan, T., 2006. Single-grain, microfloc and macrofloc volume variations observed with a lisst-100 and a digital flocculation camera. *Journal of Sea Research* 55, 87–102, doi:10.1016/j.seares.2005.09.003.
- 875  
876  
877
- 878 Moore, R., Wolf, J., Souza, A., Flint, S., 2009. Morphological evolution of

- 879 the dee estuary, eastern irish sea, uk: A tidal asymmetry approach. *Geo-*  
880 *morphology* 103, 588–596, doi:10.1016/j.geomorph.2008.08.003.
- 881 Mori, N., Suzuki, T., Kakuno, S., 2007. Noise of acoustic doppler velocime-  
882 ter data in bubbly flows. *Journal of Engineering Mechanics* 133, 122–125,  
883 doi:10.1061/(ASCE)0733-9399(2007)133:1(122).
- 884 Polton, J., Palmer, M., Howarth, M., 2011. Physical and dynamical oceanog-  
885 raphy of Liverpool Bay. *Ocean Dynamics* 61, 1421–1439.
- 886 Puls, W., Kuehl, H., Heymann, K., 1988. Settling velocity of mud flocs:  
887 results of field measurements in the Elbe and the Weser Estuary. In:  
888 Dronkers, J., van Leussen, W. (Eds.), *Physical Processes in Estuaries*.  
889 Springer-Verlag, p. 560.
- 890 Ramírez-Mendoza, R., Souza, A., Amoudry, L., 2014. Modeling flocculation  
891 in a hypertidal estuary. *Ocean Dynamics* 64, 301–313, dOI 10.1007/s10236-  
892 013-0675-4.
- 893 Reynolds, R. A., Stramski, D., Wright, V. M., Woźniak, 2010. Measurements  
894 and characterization of particle size distribution in coastal waters. *Journal*  
895 *of Geophysical Research* 115, 1–19.
- 896 Sanford, L., Maa, J.-Y., 2001. A unified erosion formulation for fine sedi-  
897 ments. *Marine Geology* 179 (1-2), 9–23.
- 898 Simpson, J., Sharples, H., 1991. *Coastal and Estuarine Studies. Dynamics*  
899 *and Exchange in Estuaries and the Coastal Zone*. American Geophysical  
900 Union, Ch. 6. Dynamically-active models in the prediction of estuarine  
901 stratification, pp. 101–113.

- 902 Son, M., Hsu, T., 2011. The effects of flocculation and bed erodibility on  
903 modeling cohesive sediment resuspension. *Journal of Geophysical Research*  
904 116 (C03021), 1–18.
- 905 SonTek, 2002. SonTek ADVField Acoustic doppler Velocimeter Technical  
906 Documentation.
- 907 Soulsby, R., 1993. Wave-current interaction within and outside the bottom  
908 boundary layer. *Coastal Engineering* 21 (1-3), 41–69.
- 909 Souza, A., Bolaños, R., Wolf, J., Prandle, D., 2011. Measurement Tech-  
910 nologies: Measure What, Where, Why, and How? Vol. 2 of *Treatise on*  
911 *Estuarine and Coastal Science*. Waltham: Academic Press., pp. 361-394.
- 912 Souza, A. J., Lane, A., 2013. Effects of freshwater inflow on sediment trans-  
913 port. *Journal of Operational Oceanography* 6 (1), 27–31.
- 914 Stanev, E., Wolff, O., Brink-Spalink, G., 2006. On the sensitivity of the  
915 sedimentary system in the East Frisian Wadden Sea to sea-level rise  
916 and wave-induced bed shear stress. *Ocean Dynamics* 56, 266–283, DOI  
917 10.1007/s10236-006-0061-6.
- 918 Strom, K., Keyvani, A., 2011. An explicit full-range settling velocity equa-  
919 tion for mud flocs. *Journal of Sedimentary Research* 81, 921–934, DOI:  
920 10.2110/jsr.2011.62.
- 921 Tennekes, H., Lumley, J., 1972. *A First Course in Turbulence*. The Mas-  
922 sachusetts Institute of Technology.

- 923 Thurston, W., 2009. Turbulence as a mediator of processes in a macrotidal  
924 estuary. Ph.D. thesis, University of Leeds, School of Earth and Environ-  
925 ment, Leeds, UK.
- 926 Todd, D., 2014. Temporal variability of suspended particulate matter in a  
927 tidal estuary. Ph.D. thesis, University of Bangor, Bangor, UK.
- 928 Trowbridge, J., 1998. On a technique for measurement of turbulent shear  
929 stress in the presence of surface waves. *Journal of Atmospheric and Ocean  
930 Technology* 15 (1), 290–298.
- 931 Turner, A., Millward, G., Tyler, A., 1994. The distribution and chemical  
932 composition of particles in a macrotidal estuary. *Estuarine, Coastal and  
933 Shelf Science* 38, 1–17.
- 934 van Leussen, W., 1994. Estuarine macroflocs and their role in fine-grained  
935 sediment transport. Ph.D. thesis, University of Utrecht, The Netherlands.
- 936 van Leussen, W., 1999. The variability of settling velocities of suspended fine-  
937 grained sediment in the Ems estuary. *Journal of Sea Research* 41, 109–118.
- 938 Verney, R., Lafite, R., Brun-Cottan, J., Le Hir, P., 2011. Behaviour of a floccu-  
939 lation during a tidal cycle: laboratory experiments and numerical  
940 modelling. *Continental Shelf Research* 31, S64–S83.
- 941 Voulgaris, G., Trowbridge, J., 1998. Evaluation of the acoustic doppler ve-  
942 locimeter (adv) for turbulence measurements. *Journal of Atmospheric and  
943 Ocean Technology* 15 (1), 272–289.

- 944 Wang, Y., Voulgaris, G., Li, Y., Yang, Y., Gao, J., Chen, J., Gao, S., 2013.  
945 Sediment resuspension, flocculation, and settling in a macrotidal estuary.  
946 Journal of Geophysical Research 118, 5591–5608, i:10.1002/jgrc.20340.
- 947 Wiberg, P., Sherwood, C., 2008. Calculating wave-generated bottom orbital  
948 velocities from surface-wave parameters. Computers & Geosciences 34,  
949 1243–1262, doi:10.1016/j.cageo.2008.02.010.
- 950 Winterwerp, J. C., 1998. A simple model for turbulence induced flocculation  
951 of cohesive sediment. Journal of Hydraulic Research 36, 309–326.
- 952 Winterwerp, J. C., 2002. On the flocculation and settling velocity of estuarine  
953 mud. Continental Shelf Research 22, 1339–1360.
- 954 Winterwerp, J. C., Manning, A. J., Martens, C., de Mulder, T., Vanlede, J.,  
955 2006. A heuristic formula for turbulence-induced flocculation of cohesive  
956 sediment. Estuarine, Coastal and Shelf Science 68, 195–207.
- 957 Winterwerp, J. C., van Kesteren, W. G. M., 2004. Introduction to the physics  
958 of cohesive sediment in the marine environment, 1st Edition. Elsevier, B.  
959 V., Amsterdam, The Netherlands.

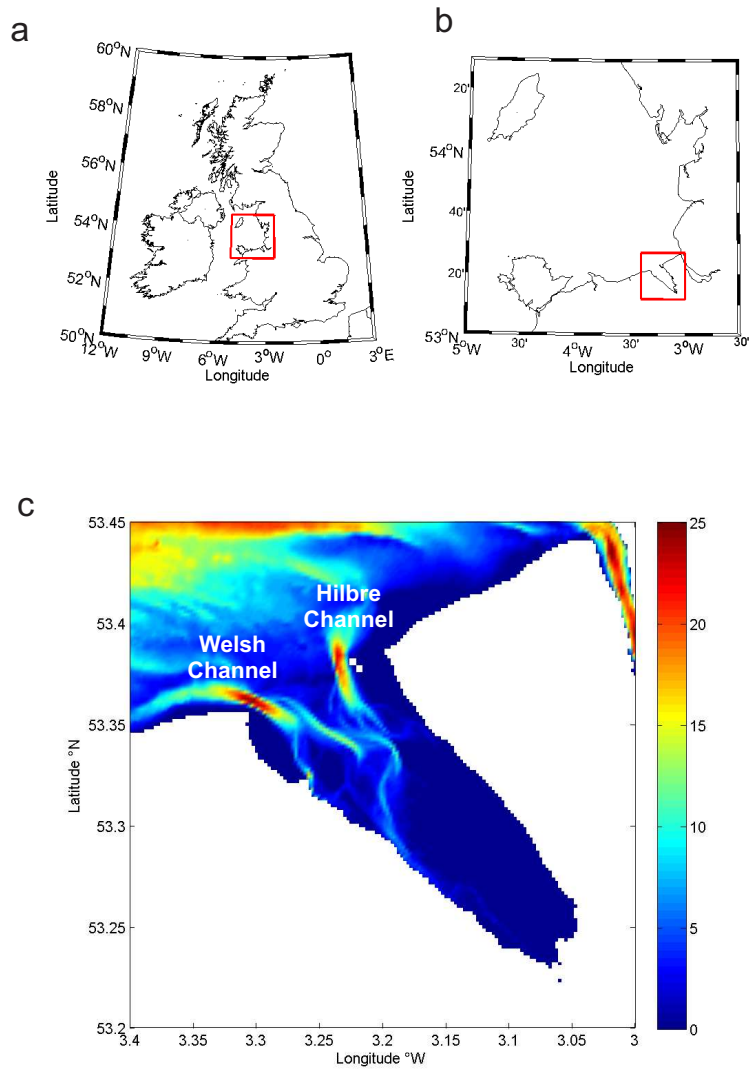


Figure 1: Location of the study site. a) United Kingdom, Liverpool Bay in red square, b) Liverpool Bay with the Dee Estuary in red square, and c) Dee Estuary, channels, Welsh to the west and Hilbre to the east of the entrance, and depth in metres.

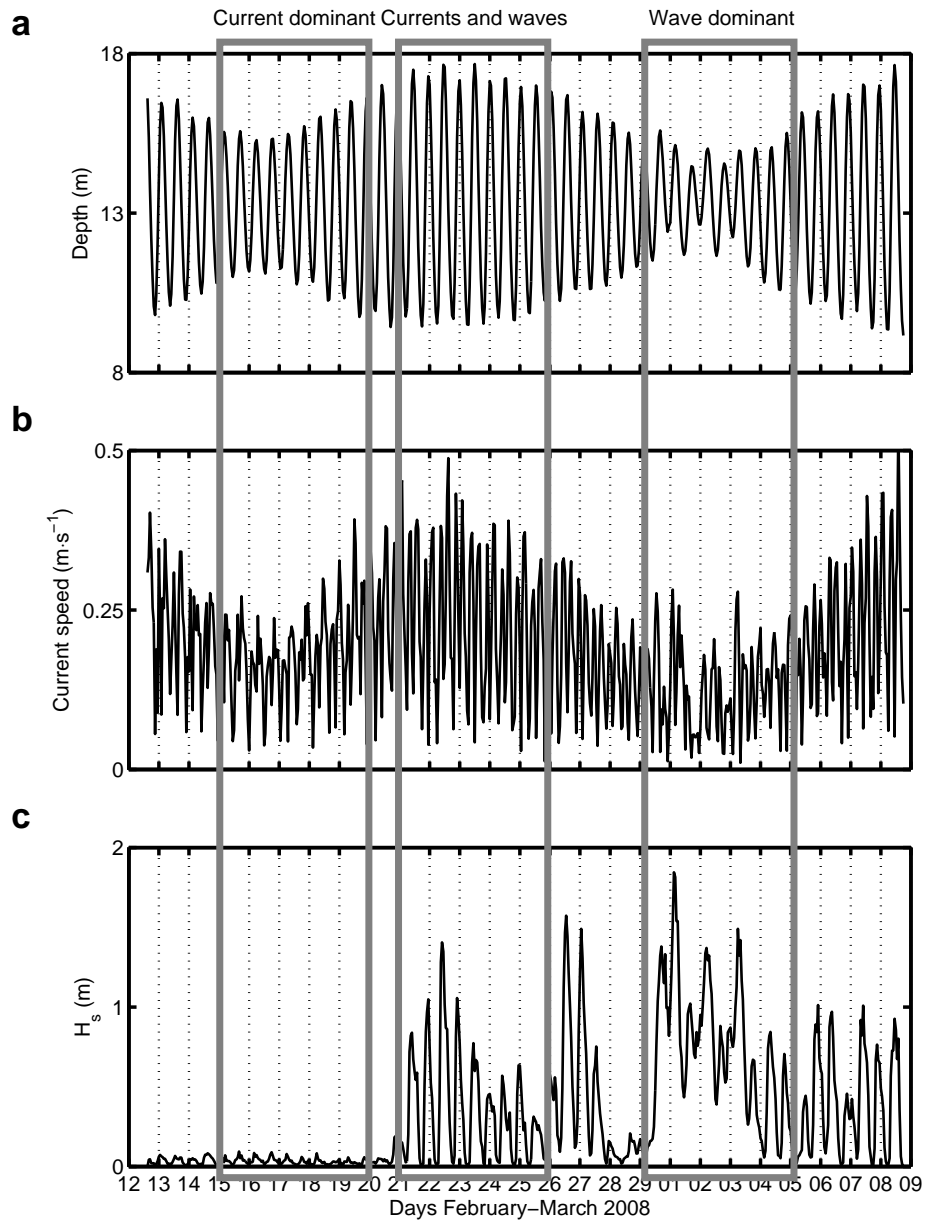


Figure 2: Separation of observations into three hydrodynamic regimes marked with grey rectangles. a) Water depth, b) horizontal bed current speed, c) significant wave height  $H_s$ .

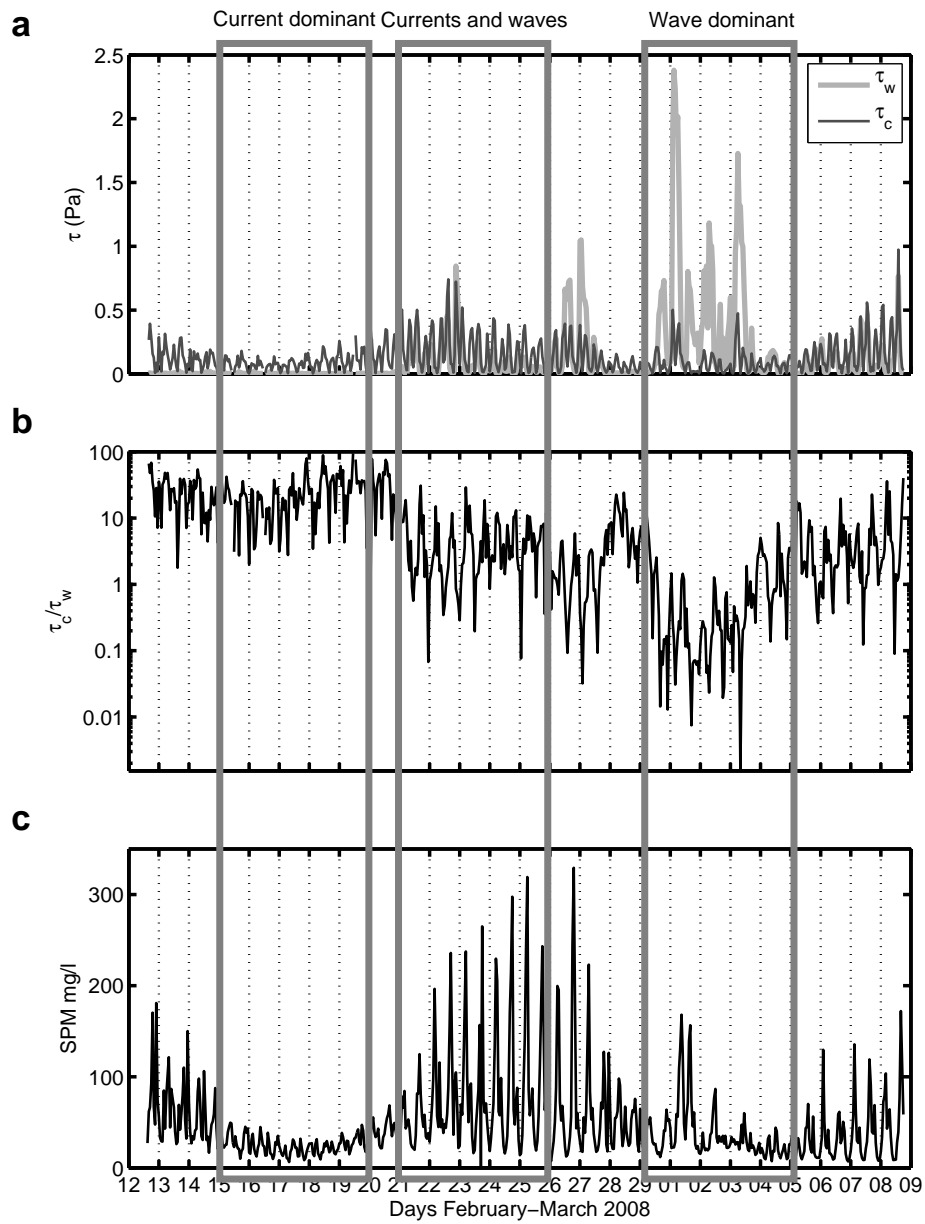


Figure 3: Shear stresses and suspended sediments during the three regimes. a) Shear stresses from currents  $\tau_c$  and waves  $\tau_w$ , b) ratio between  $\tau_c$  and  $\tau_w$ , and c) suspended particulate matter **concentration**.

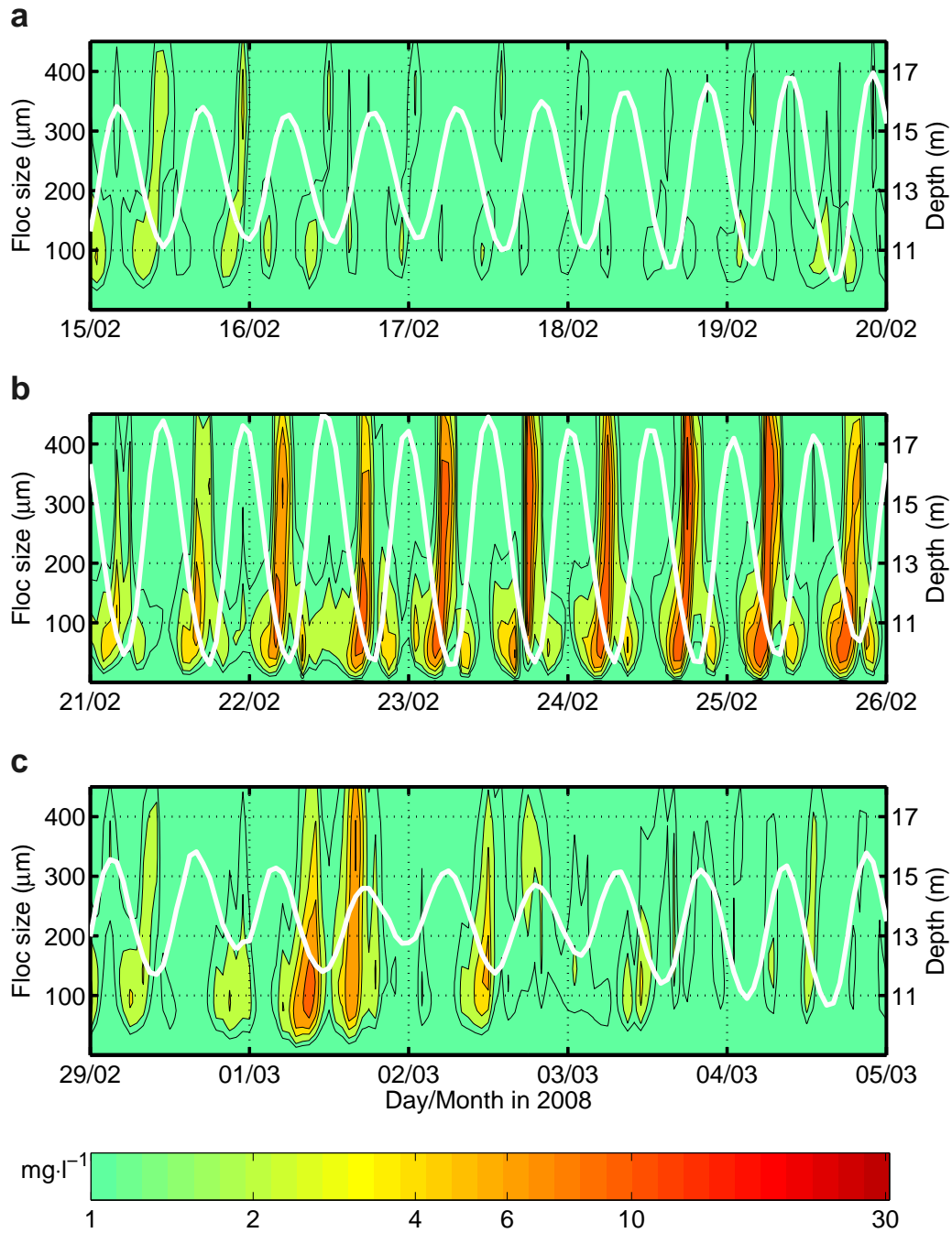


Figure 4: Floc size spectrum for the three regimes as measured by the LISST and water depth (white line). a) "current-dominant" regime, b) "currents-waves" regime, and c) "wave-dominant" regime.

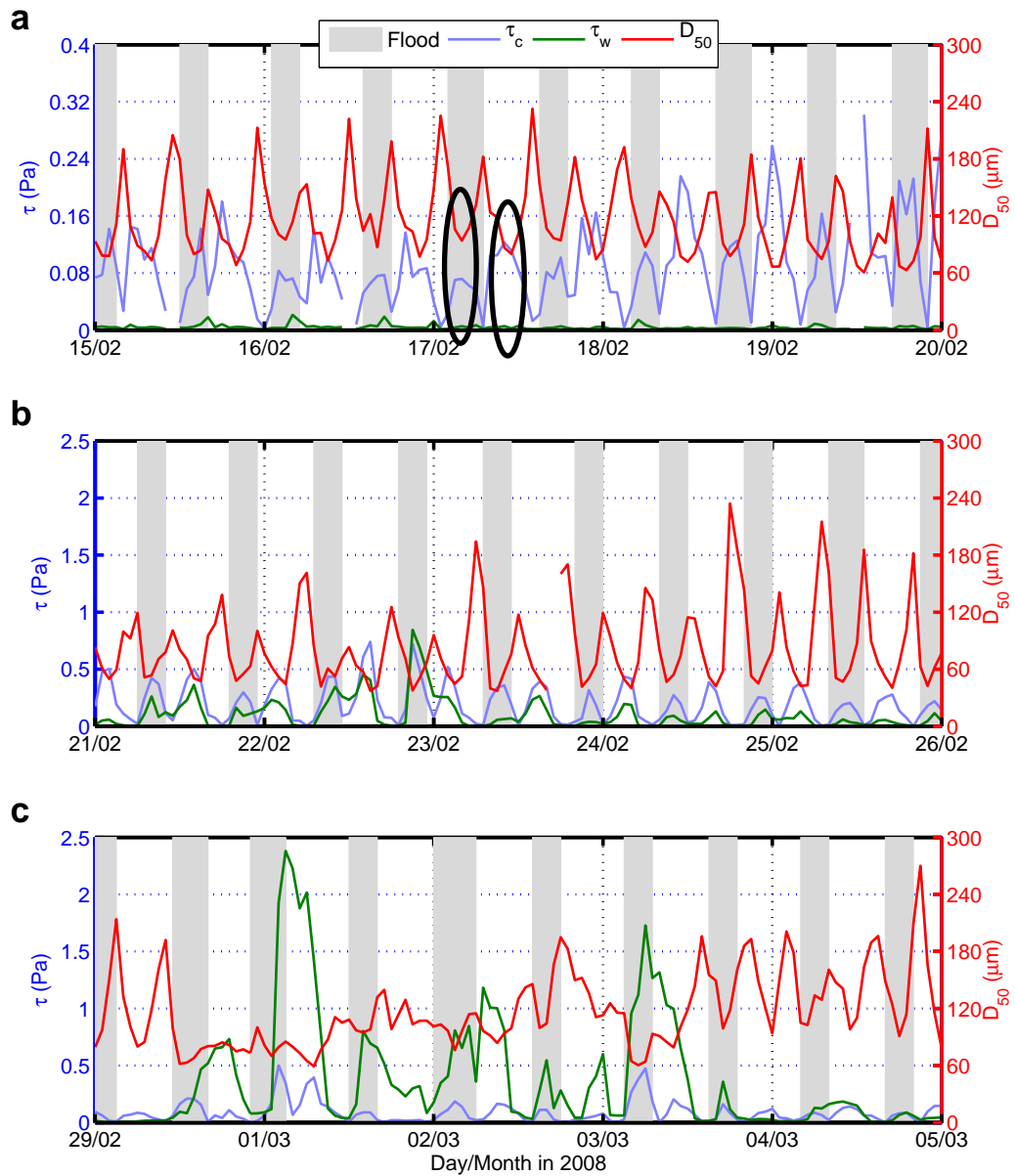


Figure 5: Shear stress from currents ( $\tau_c$ ), waves ( $\tau_w$ ), and median floc sizes ( $D_{50}$ ) for each hydrodynamic regime: a) “current-dominant”, ellipses denote an example of asymmetries in shear stress maxima and floc size minima, b) “currents-waves” and c) “wave-dominant”. Note the change in shear stress vertical scale in (a).

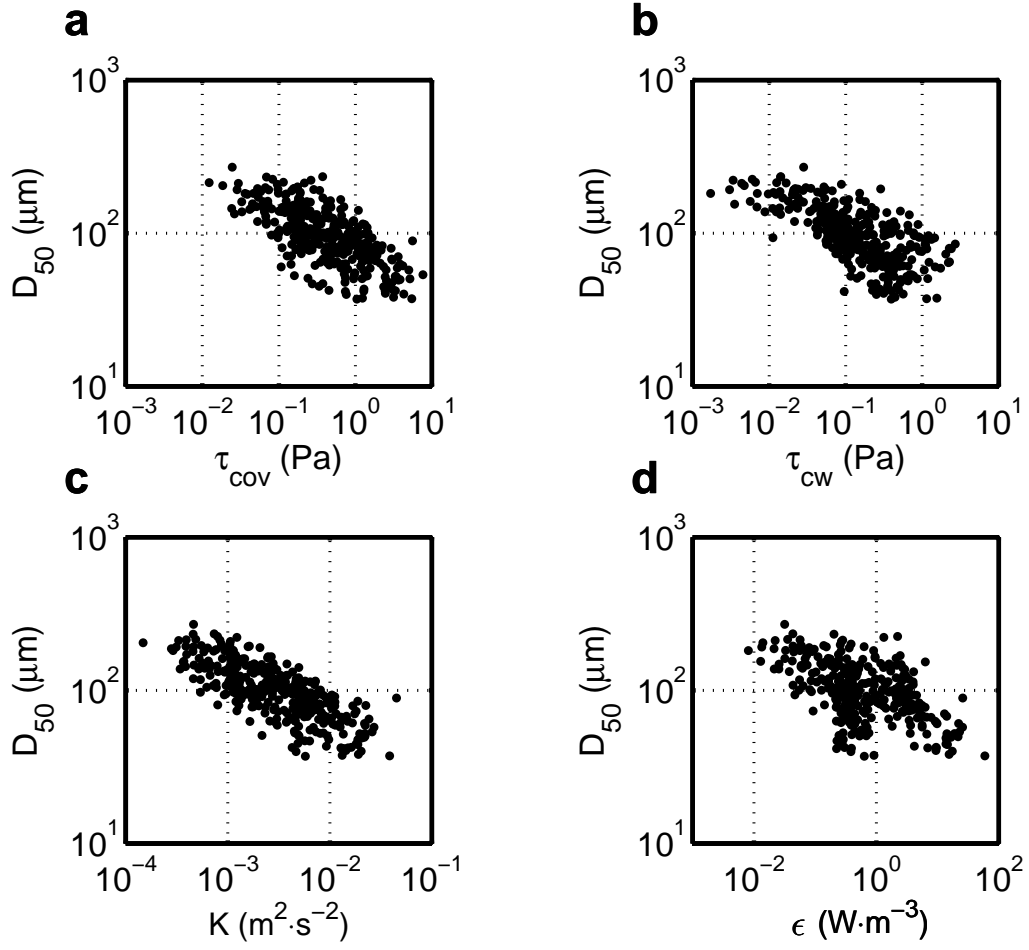


Figure 6: Dispersion diagram comparison showing the relationship of different turbulent variables with median floc size ( $D_{50}$ ) for the entire data set: a) turbulent stress using the covariance method ( $\tau_{cov}$ ), b) maximum bed shear stress from the currents and waves analysis ( $\tau_{cw}$ ), c) effective kinetic energy ( $K$ ) values from Reynolds decomposition of the current velocity record, and d) dissipation of turbulent kinetic energy ( $\epsilon$ ) from the turbulent spectrum analysis.

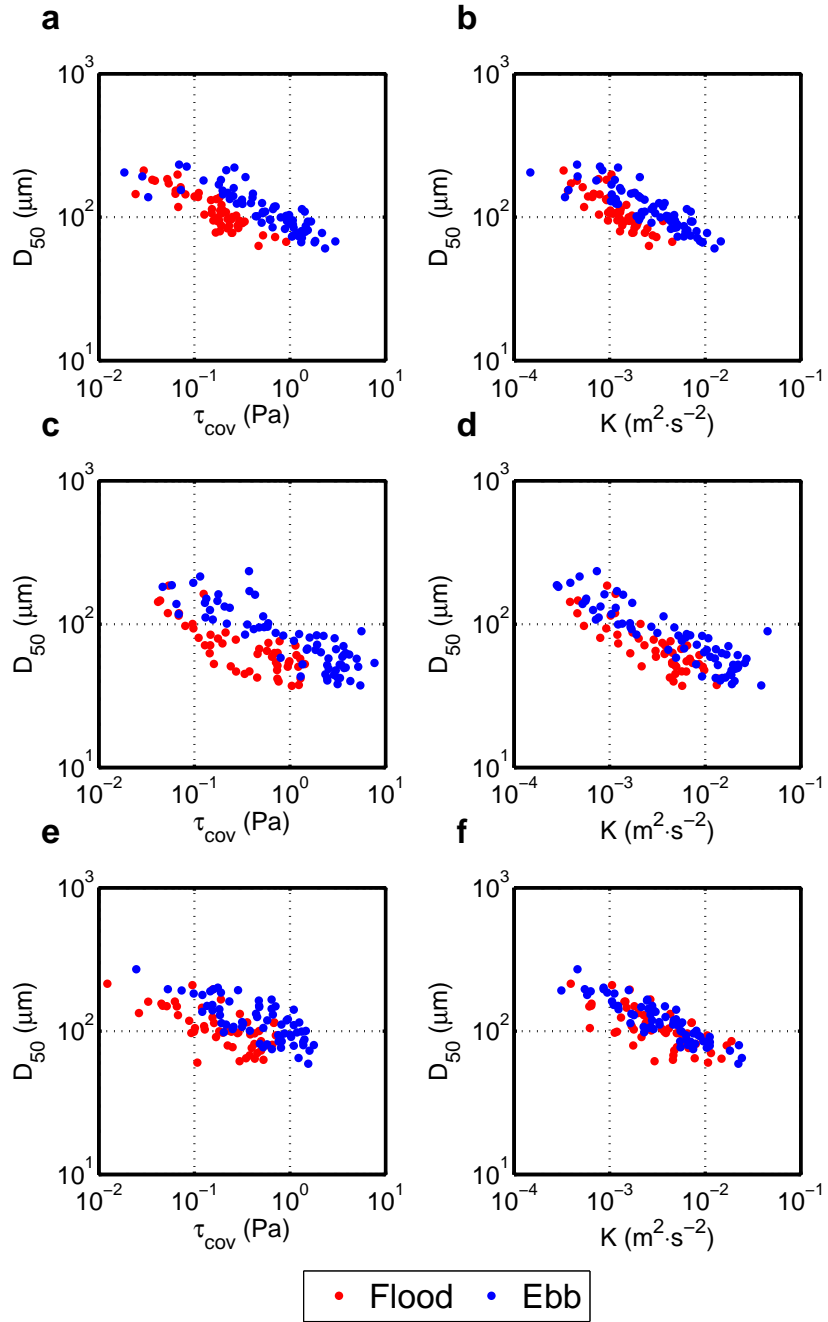


Figure 7: Median floc size as a function of shear stress from the covariance method  $\tau_{cov}$  and  $K$  for the three regimes and tidal phases: a) and b) “current-dominant”, c) and d) “currents-waves”, e) and f) “wave-dominant”.

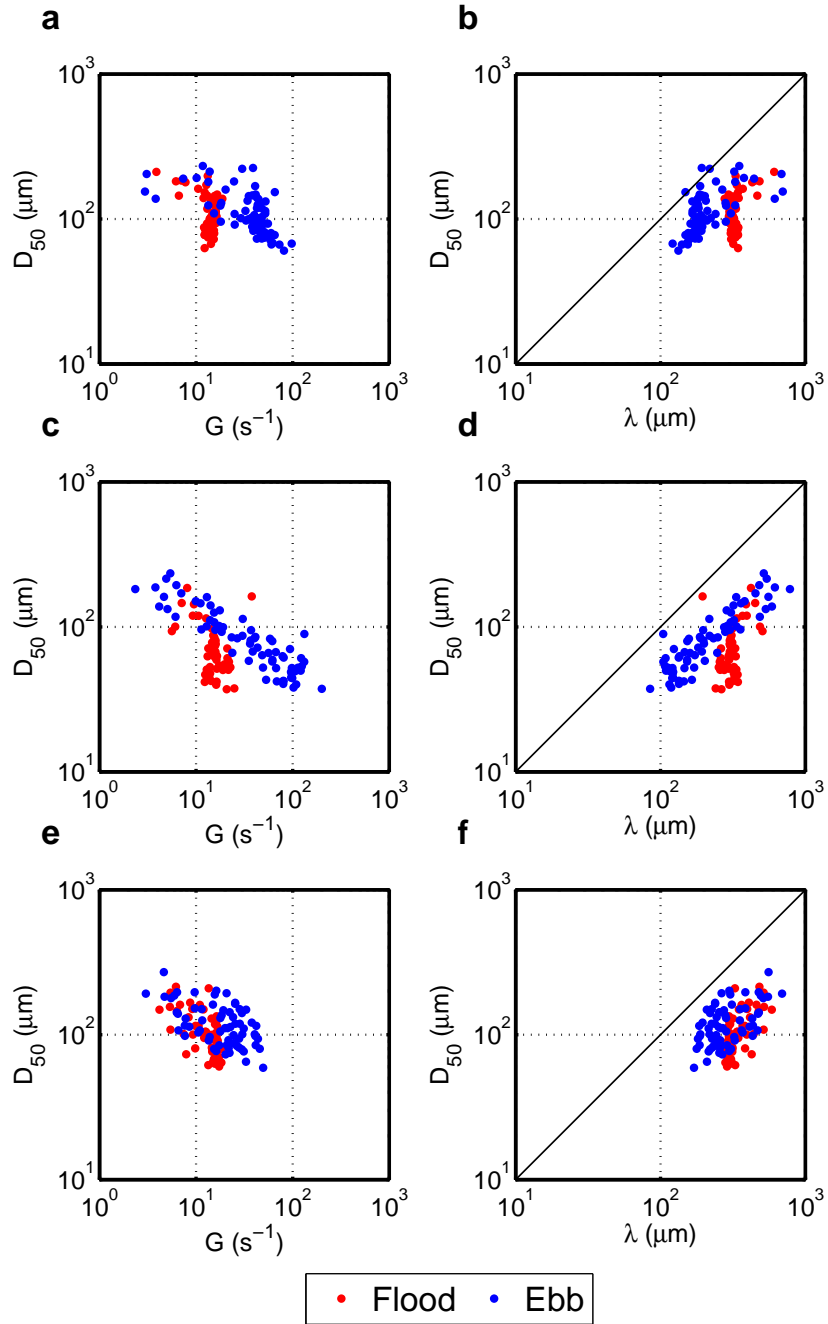


Figure 8: Median floc size  $D_{50}$  against turbulent shear rate  $G$  and Kolmogorov microscale  $\lambda$  for the three regimes and tidal phases: a) and b) “current-dominant”, c) and d) “currents-waves”, e) and f) “wave-dominant”.

Table 1: Comparison of coefficients resulting of curve fittings of the forms  $D_{50}=A \cdot (K)^B$  and  $D_{50}=A \cdot (\tau_{cov})^B$  to distributions in figure 7.  $R^2$ : determination coefficient. RMSE: Root Mean Square Error.

		$K$			$\tau_{cov}$		
		Flood	Ebb	Flood and Ebb	Flood	Ebb	Flood and Ebb
<b>Current dominant</b>	A	7.06	18.33	21.89	59.14	93.37	87.21
	B	-0.41	-0.31	-0.26	-0.34	-0.27	-0.20
	$R^2$	0.66	0.75	0.55	0.77	0.73	0.51
	RMSE	113.3	116.4	113.9	113.7	115.6	113.2
<b>Currents - waves</b>	A	8.97	15.46	14.56	48.87	78.31	66.44
	B	-0.35	-0.31	-0.29	-0.29	-0.30	-0.23
	$R^2$	0.70	0.80	0.67	0.63	0.73	0.48
	RMSE	71.2	87.0	79.3	70.2	84.5	76.47
<b>Wave dominant</b>	A	26.10	21.65	23.71	71.57	94.72	89.82
	B	-0.24	-0.30	-0.27	-0.23	-0.26	-0.18
	$R^2$	0.47	0.81	0.62	0.44	0.55	0.32
	RMSE	106.8	121.5	114.6	106.5	119.4	112.4
<b>All data</b>	A	17.81			77.68		
	B	-0.29			-0.24		
	$R^2$	0.58			0.48		
	RMSE	101.9			100.3		

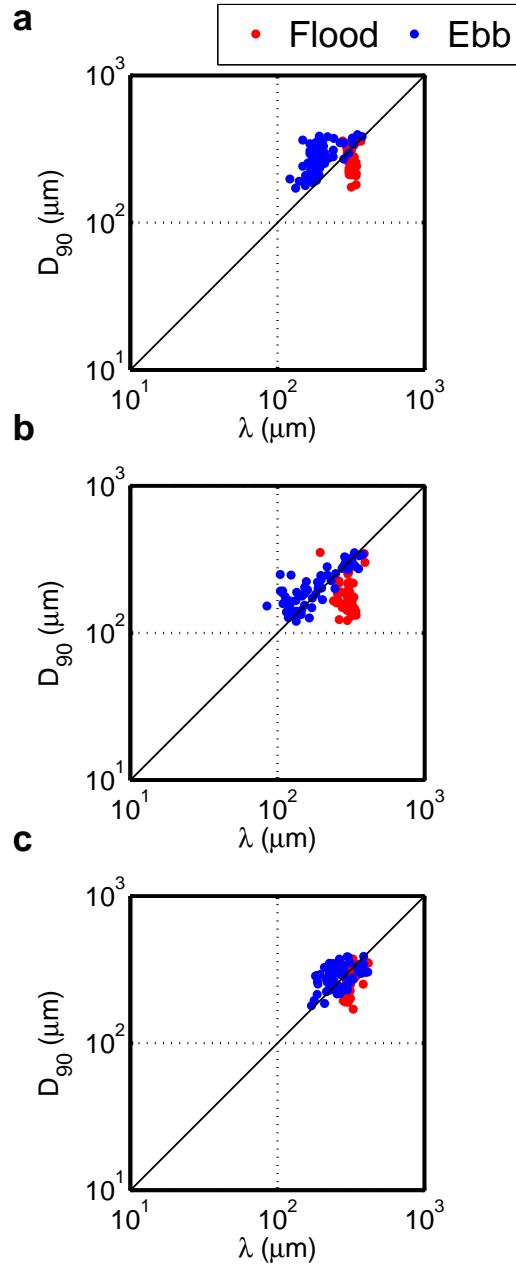


Figure 9: Kolmogorov microscale  $\lambda$  and  $D_{90}$  relationships for the three regimes and tidal phases: a) “current-dominant”, b) “currents-waves”, and c) “wave-dominant”. Axes scaling have been kept as in figure 8 for comparison.

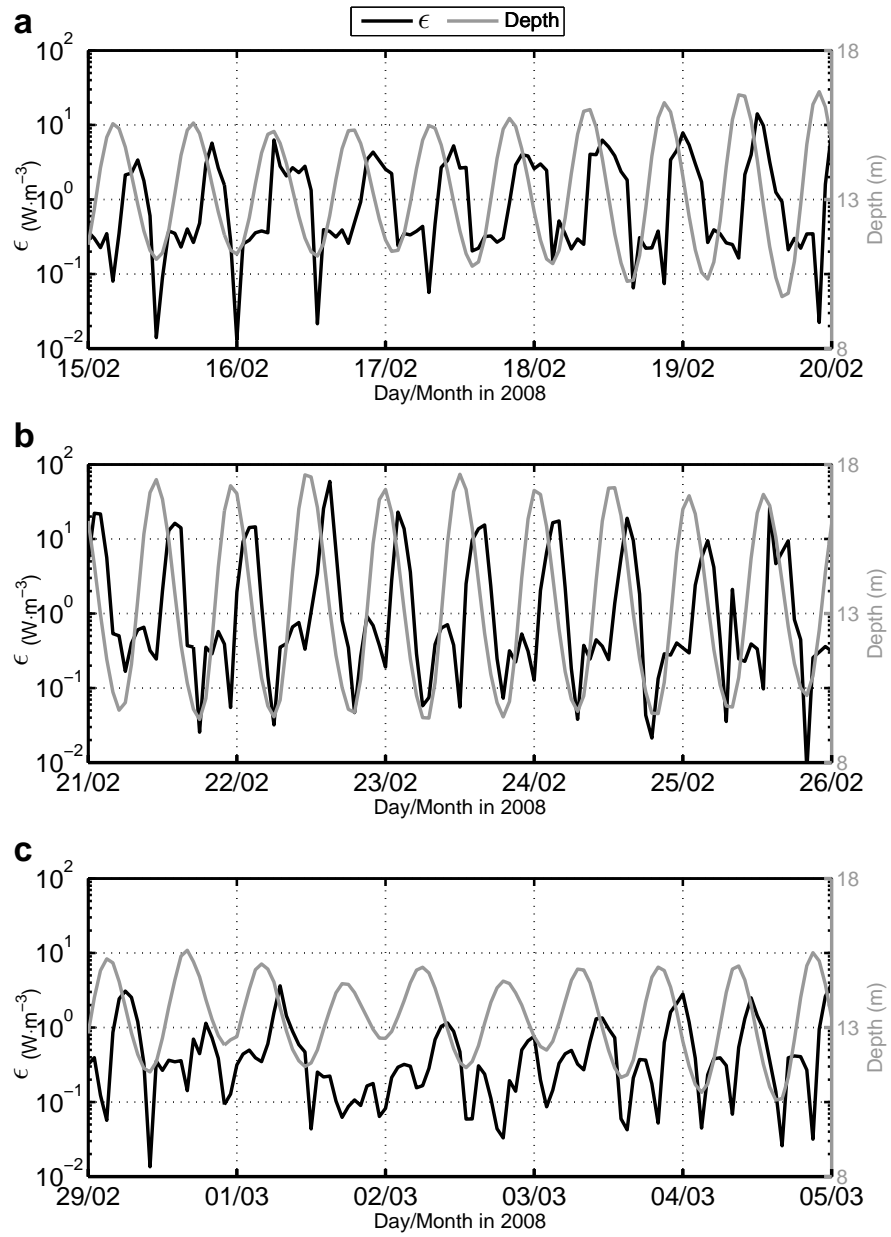


Figure 10: Time series of dissipation of turbulent kinetic energy  $\epsilon$  for the three regimes: a) “current dominant”, b) “currents-waves”, and c) “wave-dominant”.

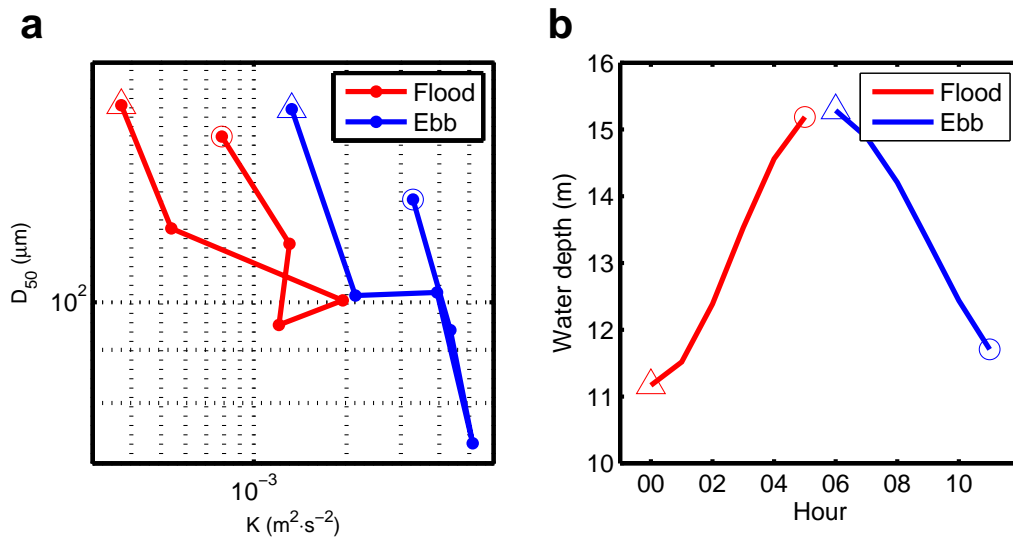


Figure 11: a) Hysteresis effect in the relationship between  $K$  and median floc size during a tidal cycle on 16 February 2008, and b) corresponding depth during the tidal cycle. Triangles and circles mark the start and end of each phase, respectively.